inorganics

MDPI

Review

Recent Advances and Challenges in Hybrid Supercapacitors Based on Metal Oxides and Carbons

Lili Gao [1,*], Fuyuan Liu [1], Jiaxing Qi [2,3], Wenyue Gao [4] and Guobao Xu [2,3,*]

[1] School of Materials Science and Engineering, Shenyang Jianzhu University, Shenyang 110168, China; fuyuanliu8895@163.com
[2] State Key Laboratory of Electroanalytical Chemistry, Changchun Institute of Applied Chemistry, Chinese Academy of Sciences, Changchun 130022, China; jiaxingq@ciac.ac.cn
[3] School of Applied Chemistry and Engineering, University of Science and Technology of China, Hefei 230026, China
[4] Institute of Marine Science and Technology, Shandong University, Qingdao 266237, China; gaowy@email.sdu.edu.cn
* Correspondence: liligao@sjzu.edu.cn (L.G.); guobaoxu@ciac.ac.cn (G.X.)

Abstract: Hybrid supercapacitors (HSCs) are a novel type of supercapacitor composed of battery-type electrodes and capacitor-type electrodes, which have directly transformed the global energy landscape. On one hand, they can replace clean energy sources that are heavily dependent on climatic conditions in specific regions, thereby enhancing the effective utilization of intermittent energy sources. On the other hand, with their high energy density akin to secondary batteries and the long lifespan and high power density characteristic of supercapacitors, they perfectly bridge the gap between secondary batteries and supercapacitors. This article reviews the fundamental energy storage principles of HSCs and highlights the latest optimization strategies for HSCs based on transition metal oxides (TMOs) and carbon over the past two years. These strategies include heteroatom doping, heterostructured materials, nanocomposites, and metal–organic frameworks (MOF). Finally, prospects on future research directions of HSCs are discussed.

Keywords: hybrid supercapacitor; metal oxides; carbon-based electrodes

check for updates

Academic Editors: Ting Deng and Jun Yan

Received: 14 January 2025
Revised: 3 February 2025
Accepted: 6 February 2025
Published: 8 February 2025

Citation: Gao, L.; Liu, F.; Qi, J.; Gao, W.; Xu, G. Recent Advances and Challenges in Hybrid Supercapacitors Based on Metal Oxides and Carbons. *Inorganics* **2025**, *13*, 49. https://doi.org/10.3390/inorganics13020049

Copyright: © 2025 by the authors. Licensee MDPI, Basel, Switzerland. This article is an open access article distributed under the terms and conditions of the Creative Commons Attribution (CC BY) license (https://creativecommons.org/licenses/by/4.0/).

1. Introduction

The rapid development of society and the swift growth of the global population have led to a continuous increase in energy demand. Environmental pollution, ecological destruction, and energy shortages have become immense challenges facing human development today [1,2]. By 2050, the energy demand is projected to be more than double the current levels [3]. Currently, 80% of global energy supply is derived from non-renewable fossil fuels, including coal, oil, and natural gas. The use of these fossil fuels not only produces harmful and toxic gasses such as SO_2 and NO but also takes millions of years or even longer to regenerate [4,5]. Renewable energy sources like solar and wind power are intermittent and their power generation conditions vary, rendering them unsuitable for direct energy supply in power grids [6,7]. Therefore, converting other energy sources into electricity and supplying it to different energy-demanding applications has become an inevitable trend in energy development [8,9]. Searching for new, renewable energy sources that can replace traditional fossil fuels, and developing novel energy storage devices with high power and energy density has become one of the crucial challenges that humanity must address in the future for the storage and transportation of electrical energy [10,11].

Based on the current status of energy storage devices, secondary batteries possess a considerable energy density that can meet the pursuit of energy [12]. However, the power density of conventional batteries is relatively low, failing to meet the requirements of applications that necessitate high power density devices [13]. While traditional capacitors have a notable power density, their energy density is very low, making it challenging for them to become the energy storage devices needed for the future [14]. Encouragingly, the recently emerged hybrid ion capacitors represent a new type of supercapacitor that has directly changed the global energy landscape. On one hand, they can replace clean energy sources that are heavily dependent on weather conditions in specific regions, thereby enhancing the effective utilization of intermittent energy sources. On the other hand, with the high energy density of secondary batteries and the long lifespan and high power density of supercapacitors, they perfectly bridge the gap between the two [15–17]. Furthermore, to cater to the growing human living demands, HSCs hold immense industrial potential in applications such as electric vehicles, renewable energy sources (solar and wind power), wearable devices, and electronic products [18–22]. In applications such as new energy vehicles, large-scale medical devices, and heavy-duty machinery, energy storage devices with superior low-temperature performance and excellent instantaneous power characteristics are required during rapid startups. However, the impact of instantaneous high-current discharge, particularly in outdoor environments at −20 °C in northern regions, can significantly shorten the lifespan of storage batteries. During battery replacement in charging stations and commercial payment terminals, it is necessary to supplement the backup power supply to ensure data protection in the event of power failure, and the HSC batteries are well-suited to meet these demands. Therefore, designing and preparing high-performance electrode materials is key to improving the performance of hybrid ion capacitors, with common materials including conductive polymers [23], carbon materials [24], metal oxides [25], and metal sulfides [26]. Among these, transition metal oxides (TMOs), such as nickel oxide [27], iron oxide [28], cobalt oxide [29], zinc oxide [30], and manganese dioxide [31], are widely used as battery-type electrode materials due to their variable oxidation states, environmental friendliness, high specific capacity, and long lifespan. However, poor conductivity and slow charge transfer have limited the practical applications of TMOs. Furthermore, carbon materials generally exhibit behaviors related to pure non-Faradaic reactions, akin to Electric Double Layer Capacitors (EDLC) or pseudocapacitance, and are commonly used as electrodes in hybrid ion capacitors. However, the performance of carbon-based electrode materials is less than ideal, with their energy density, particularly the volumetric energy density, being low. This hinders the simultaneous achievement of high energy and power densities, severely limiting their practical applications in the field of energy storage.

In recent years, due to the unresolved economic aspects of HSC production and the enhancement of energy density/power density/specific capacity/safety, fastcharge–discharge rates, excellent cycling stability, and high rate capability have garnered significant attention from researchers to enhance capacitance and energy density. To address these issues and to assist a broad and interdisciplinary readership in deeper research within this field, this paper reviews the energy storage principles of hybrid supercapacitors, with a focus on HSCs based on TMOs and carbon. It highlights the latest optimization strategies, including heteroatom doping, heterostructures, nanocomposites, metal–organic frameworks, and electrolytes. Finally, the paper discusses and prospects future research directions and possibilities in this field.

2. Composition and Energy Storage Mechanism of HSC

HSC are primarily composed of current collectors, electrolytes, separators, and electrodes. The current collectors not only serve as a repository for electrons but also act as a substrate that allows for the uniform distribution of the electrode material on their surface. The electrolyte, separator, and electrodes are the core components that directly determine the performance of the device. The electrolyte, positioned between the anode and cathode, facilitates the transport and conduction of ions [32–34]. Typically, electrolytes should possess chemical and electrochemical stability, sufficient ion conductivity, and good thermodynamic stability. Therefore, electrolytes are pivotal in enhancing the electrochemical performance of HSC, directly influencing their energy density, power density, specific capacity, and safety. The impact of electrolytes on the performance of HSC under various conditions has been extensively studied and reviewed by researchers [35]. Electrolytes are generally categorized into four types: aqueous electrolytes, organic electrolytes, solid or quasi-solid electrolytes, and ionic liquid electrolytes [36]. Among these, aqueous electrolytes are widely used due to their low cost, simple preparation methods, high ionic conductivity, and superior safety. However, the electrochemical stability window of aqueous electrolytes is limited by the decomposition voltage of water [37]. Organic electrolytes offer a wider electrochemical stability window (>3.0 V), but their practical application is constrained by flammability, high cost, and low ionic conductivity [38]. Compared to organic electrolytes, ionic liquid electrolytes not only provide a comparable wide electrochemical stability window but are also safer and more environmentally friendly. Nevertheless, the high viscosity of ionic liquids often results in lower ionic conductivity. Additionally, both ionic liquids and organic electrolytes require an absolutely anhydrous environment and involve complex purification and drying procedures that increase costs. The large-scale application of these electrolytes still faces significant challenges. On the other hand, hydrogel electrolytes exhibit superior mechanical properties and perform well at lower temperatures. In the realm of solid electrolytes, gel polymer electrolytes, which exist in a liquid phase within a solid matrix, dominate the market due to their high ionic conductivity [39]. In these systems, a polymer framework serves as the support, with electrolyte salts and plasticizers uniformly distributed within the polymer network. Commonly used polymers include polyethylene oxide (PEO), polyvinyl alcohol (PVA), polyacrylic acid (PAA), and polyacrylamide (PAMM), among others. The separator is a film that allows only target ions to pass freely, and it must have stable physical and chemical properties to prevent contact between the anode and cathode. [40].

In fact, charge storage is achieved through two distinct mechanisms: the physical adsorption/desorption of ions on the surface of capacitor-type electrode materials and the battery-type Faradaic reactions in battery-type electrodes.

Carbon–based materials can be used as capacitor-type anodes or cathodes, with their energy storage mechanism primarily based on EDLC (Figure 1a). During the charge process, electrons reach the anode through the external circuit, under the influence of the applied electric field, free ions with opposite charges migrate to the surface of the carbon–based material. Then, via electrostatic interactions, an electric double layer spontaneously forms at the interface between the electrode and electrolyte, leading to electrochemical dynamic equilibrium [41]. During the discharge process, electrons and ions desorb through electrostatic interactions, and the cations and anions desorb from carbon materials [42]. In the case of zinc-ion hybrid capacitor, the energy storage mechanism of the carbon-based cathode is mainly based on EDLC. For cation adsorption/desorption, the interaction

equation is as shown in Equation (1), while for anion (X^-) adsorption/desorption, the interaction equation is as shown in Equation (2) [43].

$$C + Zn^{2+} \rightleftharpoons C||Zn^{2+} \quad (1)$$

$$C + X^- \rightleftharpoons C||X^- \quad (2)$$

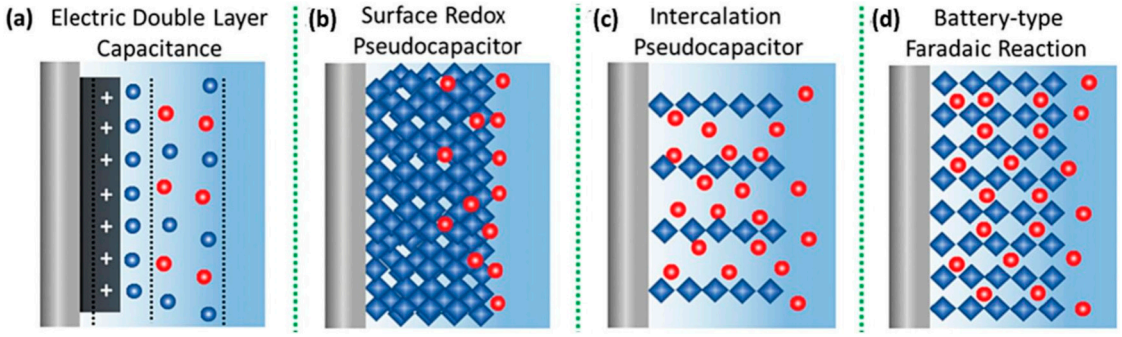

Figure 1. Energy storage mechanism of (**a**) EDLC, (**b**) surface redox pseudocapacitor, (**c**) intercalation pseudocapacitor, and (**d**) battery-type Faradaic reaction. Reproduced with permission from [41].

This is a static electrochemical energy storage process in which no electrode chemical reactions occur and no induced current is produced. During the charge–discharge process, an oriented double-layer distribution of electrons and dipoles occurs at the electrode/electrolyte interface, forming a capacitor-like structure similar to traditional plate capacitors to achieve energy storage. The charge–discharge process of EDLC is a pure non-Faradaic reaction involving simple adsorption/desorption of charges carries at the electrode/electrolyte interface, which can achieve fast charging or discharging. Therefore, it immediately responds to changes in charge storage on the electrode material surface, resulting in ideal symmetric triangular curves of the constant current charge–discharge (GCD) and rectangular cyclic voltammetry (CV) curves. Furthermore, carbon-based anodes or cathodes containing oxygen-containing functional groups or doped with heteroatoms exhibit pseudocapacitive mechanisms of surface redox reactions, which simultaneously display both Faradaic and EDLC mechanisms to achieve charge storage (Figure 1b). The GCD and CV curves are very similar to those of EDLC, being quasi-rectangular and quasi-triangular. The surface redox reaction is as shown in Equation (3) [44].

$$C\text{–}O + Zn^{2+} + 2e^- \rightleftharpoons C\text{–}O + Zn \quad (3)$$

For TMOs, in addition to the pseudocapacitive surface redox reactions mentioned earlier, they sometimes also exhibit intercalation pseudocapacitive mechanisms. A key feature of intercalation pseudocapacitance is that no phase transition occurs in the material during intercalation. Compared to EDLC, the charge storage process of intercalation pseudocapacitance involves reversible Faradaic electrochemical reactions of a large number of ions at the material–electrolyte interface. In a dual-ion HSC constructed with a Ni_3S_2/Ni_2O_3 heterostructure cathode using LiOH catholyte, two pseudocapacitive mechanisms—surface redox and intercalation—are present during discharge (Figure 1c) [45], while the charging process exhibits a different type of battery-like redox reaction (Figure 1d). Unlike the storage mechanism of surface redox pseudocapacitance, the redox process of battery-type anode/cathode materials involves phase transitions and stores more charge within the electrode material, thereby further enhancing the capacitance and energy density of the hybrid sensor [46]. Additionally, the battery-like redox process introduces buffer platforms in the GCD and forms a pair of distinct redox peaks in the CV curves.

Currently, the types of HSCs based on TMOs and carbon mainly include alkali HSCs, lithium-ion HSCs (Li-HSC), sodium-ion HSCs (Na-HSC), and zinc-ion HSCs (Zn-HSC). Alkaline HSCs are generally composed of carbon-based anodes and battery-type TMO cathodes. The alkaline electrolyte effectively inhibits the hydrogen evolution reaction (HER) at the electrode interface [47], and the TMOs undergo battery-like redox reactions with OH^- in the electrolyte to store charge. The energy storage mechanism of Li-HSC primarily includes the Faradaic reactions of insertion/extraction of lithium ions (Li^+ ions) into/from the negative electrodes, conversion and alloying reactions, and the physical adsorption/desorption of ions on the surface of the capacitor-type cathode material [48–51]. However, the intercalation-type graphite anode also faces some problems, such as sluggish Li^+ diffusion kinetics, and the development of highly crystalline, anisotropic lamellar structures under low voltage conditions, leading to the inability to achieve high capacities during fast charging [52–54]. In addition, Na-HSC is similar to Li-HSC in past reports. However, due to the larger radius of Na^+ (0.98 Å), the kinetics of anodic redox reactions are sluggish, severely affecting the electrochemical performance of Na-HSC. A typical Zn-HSC generally uses zinc metal as an anode that can accommodate Zn^{2+}, which displays highly reversible Zn^{2+} plating/stripping processes during the charge and discharge process. During the charge process, Zn^{2+} in the electrolyte migrates to the anode and deposits on the zinc anode, while metallic zinc releases electrons to form Zn^{2+} ions during the discharge process. The half-reaction for this reversible redox process is presented in the following Equation (4) [55]:

$$Zn^{2+} + 2e^- \rightleftharpoons Zn \quad (4)$$

Zn-HSCs typically have cathodes composed of carbon-based materials and non-carbon-based materials such as MXenes, TMOs, and conductive polymers. Zinc has a lower redox potential (−0.76 V, versus the standard hydrogen electrode), is much less reactive, and is safer to handle. Moreover, zinc has a theoretical gravimetric capacity of 820 mAh g^{-1} and a volumetric capacity of 5855 mAh cm^{-3}, which can serve as both a current collector and active material [56]. Zinc has merits of low cost, abundance in the earth, and environmental friendliness. Therefore, Zn-HSCs are not only a potential candidate for Li-HSCs and batteries but are also capable of achieving similar energy densities, higher charge–discharge rates, higher power densities, and a long cycling life. Nevertheless, Zn-HSCs also face several challenges that need to be addressed, such as the formation of zinc dendrites on the surface of the zinc anode after subsequent cycles. The eventual cracking of these dendrites can lead to dead zinc, rendering the capacitor unable to charge and discharge, thus, reducing cycle life. Overall, the aforementioned types of HSCs all have their shortcomings, and it is crucial to adopt effective optimization strategies to improve their electrical performance. The optimization strategies for the performance of these types of ion hybrid capacitors will be elaborated in detail in the subsequent sections of this paper.

3. Index of Characteristics

Several important metrics are commonly used to evaluate their electrochemical performance.

(1) Specific capacity

Specific capacity refers to the charge storage capability of the electroactive material or the entire capacitor per unit volume (or unit mass).

(2) Specific Energy

Specific energy refers to the energy that can be stored per unit volume or unit mass of the electroactive material or capacitor.

(3) Power density

Power density refers to the rated power of an electroactive material or capacitor per unit mass or volume, and it is a physical quantity used to represent the rate of discharge.

(4) Cycle Stability

In electrochemical testing, completing one cycle of the charge and discharge process constitutes a single cycle. The cycle life of an energy storage device is measured by the retention rate of its initial specific capacitance after multiple cycles of charge and discharge.

4. Performance Optimization Strategies and Applications of HSC Based on TMOs/Carbon Materials

4.1. Atomic Doping Optimization Strategy Based on TMOs/Carbon Materials

Atomic or ionic doping, as well as co-doping, have been regarded as a promising strategy to optimizing the physical and chemical properties of electrode materials. The specific location where heteroatoms are doped plays a crucial role in determining the electrochemical performance of these materials. However, excessive concentrations of heteroatom doping can disrupt the crystallinity of materials, thereby severely compromising their cycling stability. Consequently, the development of novel selective heteroatom doping strategies is imperative. Ding et al. [57] firstly demonstrated that the doping position can be adjusted with varying the heating rate. By controlling the heating rate of the urea-assisted annealing process, the doping site of nitrogen (N) atoms in the orthogonal Nb_2O_5 (t–Nb_2O_5) crystal structure (Figure 2a) was adjusted to enhance its rate capability. The study showed that rapid heating (10 °C min^{-1}) can effectively regulate the substitution of N within the t–Nb_2O_5 lattice (Figure 2b). This process not only results in a narrowing of the bandgap but also leads to an expansion of the transport layer spacing, facilitating the movement of Li^+. The N doping sites optimized (Figure 2c) at moderate heating rates (5 °C min^{-1}) can effectively enhance the migration of Li^+ and electrons. Additionally, the interstitial N formed (Figure 2d) during slower heating rates (1 °C min^{-1}) creates an electron-rich environment, reducing the diffusion barrier of Li^+ in the layer. However, an excessive amount of interstitial N can increase the steric hindrance for Li^+ diffusion, which is not favorable for the electron enrichment of the Li^+ transport layer. Furthermore, studies have demonstrated that a slower heating rate is conducive to increasing the percentage of nitrogen doping. Due to the synergistic effects of N doping at different positions, the N–doped t–Nb_2O_5 material exhibits excellent rate performance (104.6 mA h g^{-1} at 25 °C) and 70.5% capacity retention after 1000 cycles at 5 °C. Even at a high power density of 8.4 kW kg^{-1}, the constructed lithium–ion hybrid capacitor displayed a high energy density of 46.6 Wh kg^{-1}. This strategy provides a promising and feasible approach for the precise control of heteroatom doping positions.

Recently, TMOs of elements including Mn, Nb, V, Ni, Fe, Mo, Co, etc., have secured a significant portion in the fabrication of the cathode/anode in hybrid capacitors as battery–type materials. However, pure TMOs have some drawbacks when used as materials in hybrid capacitors, such as drastic volume expansion, low electronic conductivity, irreversible structural degradation, particle aggregation, and sluggish electrochemical reaction kinetics, leading to capacity decay and poor cycling stability [58]. These challenges can be mitigated by incorporating heteroatoms, ions, and conductive polymers into TMOs [59–65].

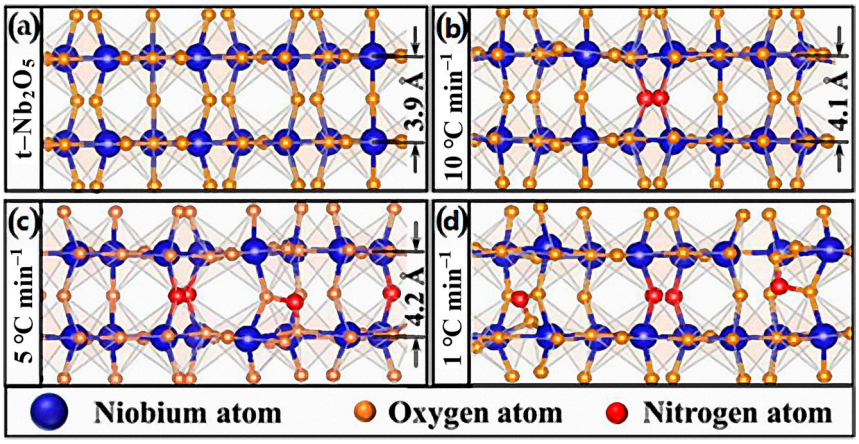

Figure 2. Schematic diagrams of N doping model of different samples, (**a**) t–Nb_2O_5, and different heating rates of (**b**) 10 °C min^{-1}, (**c**) 5 °C min^{-1}, (**d**) 1 °C min^{-1} control the doping site of N atoms in the orthogonal t–Nb_2O_5 crystal structure [57].

Manganese oxide (Mn_2O_3) is an excellent battery-type cathode material; it possesses low toxicity, environmental friendliness, cost effectiveness, superior chemical stability and electrochemical properties, a high theoretical capacity, and natural abundance. Moreover, manganese exists in various ionic states (Mn^{2+}, Mn^{3+}, Mn^{4+}, and Mn^{6+}). It can be used with several alkaline/acidic electrolytes [66–68]. Unfortunately, the high lattice energy of Mn_2O_3 nanoparticles hinders charge transport, resulting in lower charge storage capacity and conductivity. Additionally, due to phase transitions that cause continuous deformation and volume expansion at high charge–discharge rates, its electrochemical performance and durability are reduced [69,70]. Karuppaiah et al. [71] prepared neodymium (Nd)–doped α–Mn_2O_3 microspheres (MSs) with uniform morphology, high porosity, oxygen vacancies, and robust micro–nano structures using a simple hydrothermal method (Figure 3). The uniform morphology and porosity provide numerous electrochemically active sites for the insertion/deduction of OH^- ions, while Nd doping significantly increases the oxygen vacancy content in Mn_2O_3, effectively enhancing its energy density and conductivity. Furthermore, the robust micro–nano structure prevents the expansion and contraction of the active material during cycling, increasing the material's durability and lifespan. With the optimal doping condition (Nd5%–Mn_2O_3 3D–MSs), it exhibits a high specific capacitance of 862.14 F g^{-1} (431.07 C g^{-1}) at 0.5 A g^{-1} and an excellent cycle retention rate of 97.30% after 2000 cycles. Using Nd5%–Mn_2O_3 3D–MSs as a battery-type cathode and activated carbon (AC) as a capacitor-type anode, the constructed hybrid capacitor has a maximum energy density of 32.26 Wh kg^{-1} at a power density of 800 W kg^{-1}, with only a 4.56% capacity loss after 10,000 cycles, demonstrating good cycle retention performance.

The metal ion pre-intercalation doping strategy involves inserting metal cations into the layered structure of TMOs, which can effectively expand the interlayer spacing of TMOs and improve the storage performance and stability of the metal oxides [72,73]. Unfortunately, TMOs doped with single metal ions still have drawbacks such as slow electrochemical kinetics and poor conductivity. Recent studies have found that further inserting conductive polymers into TMOs based on the single metal ion doping strategy can enhance the electrochemical performance of the TMOs electrode materials. Xue et al. [74] prepared ZnxMnO_2/PPy (ZMOP) electrode materials using a hydrothermal method. The doping of Zn^{2+} and the addition of polypyrrole (PPy) enhanced the structural stability and conductivity of MnO_2. The prepared ZMOP cathode exhibited excellent specific capacity (156.4 mAh g^{-1} at 0.1 A g^{-1}) and outstanding cycle performance (82.6% retention after 5000 cycles at 0.2 A g^{-1}). Moreover, a flexible Zn-HSC was assembled using ZMOP nanowires as the cathode and PPy-derived porous carbon nanotubes (PCNTs) as the anode

materials, which showed good cycle stability. The insertion–extraction processes on the ZMOP nanowire cathode and the adsorption–desorption processes on the PCNT anode both demonstrated excellent electrochemical performance, achieving a high capacitance of 109 F g^{-1} at 0.1 A g^{-1}. Meanwhile, the corresponding energy density reached 20 Wh kg^{-1} at a power density of 867 W kg^{-1}. After 5000 cycles at 0.2 A g^{-1}, the cycle performance of the Zn-HSC remained at 86.4%. The ZMOP nanowires prepared by this strategy are potential high-performance cathode materials for constructing aqueous zinc-ion capacitors. Similarly, Xu [75] combined Co^{2+} ions and polyaniline (PANI) with V_2O (CoVO–PANI) and synthesized CoVO–PANI cathode materials (CoVO–PANI@CC) in situ on carbon cloth via a simple one-step hydrothermal method (Figure 4). A flexible zinc-ion HSC was constructed using CoVO–PANI@CC as the cathode and AC@CC as the anode. The feathery morphology of CoVO–PANI@CC provided a large surface area, which increased the contact area with the electrolyte and was beneficial for the diffusion of Zn^{2+}. The synergistic interaction between Co^{2+} and polyaniline expanded the interlayer spacing of CoVO–PANI, reduced the binding energy and diffusion barrier for Zn^{2+}, and improved the electron transport conductivity of the material. Under optimal conditions, the CoVO–PANI@CC//2 M $ZnSO_4$//AC@CC exhibited a high areal capacitance of 847.3 mF cm^{-2} at 1 mA cm^{-2}. After 2000 cycles at 50 mA cm^{-2}, the retention rate of CoVO–PANI@CC//2M $ZnSO_4$//AC@CC was 81.37%, and the coulomb efficiency was 100%. The assembled flexible Zn-HSC device maintained excellent electrochemical performance, with high flexibility and stability, and an area capacity of 775.6 mF cm^{-2} at 1 mA cm^{-2}. This strategy provides a feasible method for the application of vanadium-based cathode materials in flexible zinc-ion supercapacitors.

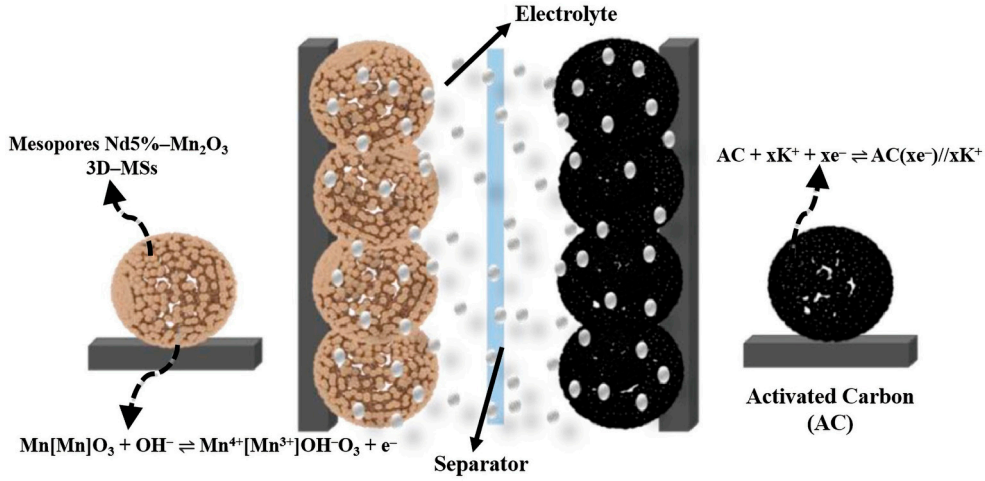

Figure 3. Schematic diagram shows the fabrication of a pouch–type HSC with mesoporous Nd5%–Mn_2O_3 3D–MSs as positive and AC as negative electrodes with filter paper as a separator in KOH electrolyte [71].

Carbon-based materials, including AC [76–78], porous carbon [79,80], graphene [81–86], carbon nanotubes (CNTs) [87–90], carbon nanofibers (CNFs) [91–93], and metal–organic framework-derived carbon [94], have been extensively studied as electrode materials for hybrid capacitors.

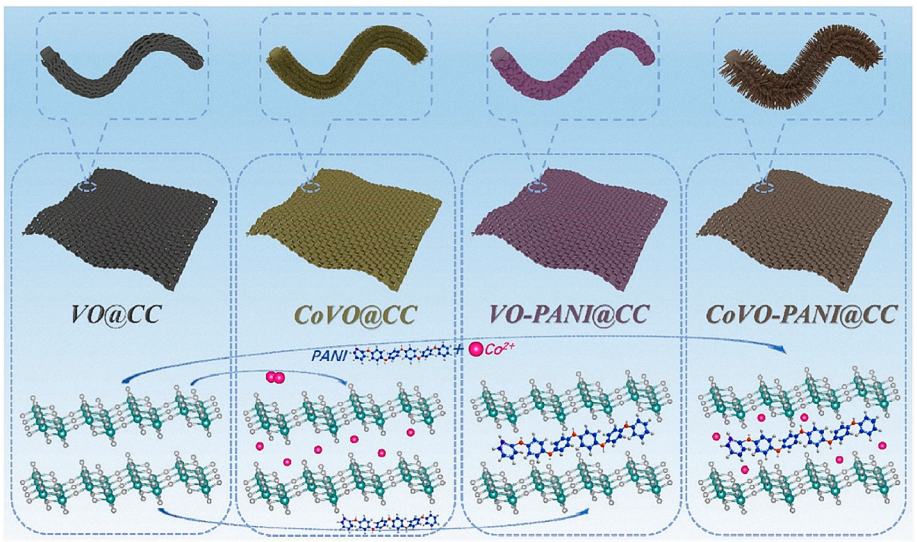

Figure 4. The preparation schematics of vo@cC, Covo@CC, VO–PANI@CC, and CoVO–PANI@CC [75].

Introducing heteroatoms (O, N, S, P, B, etc.) into the carbon matrix can improve the conductivity and surface hydrophilicity of carbon-based materials, thereby enhancing their capacitive performance. Li et al. [95] constructed a zinc-ion supercapacitor with a quadruple heteroatom self-doped hierarchical porous AC as the cathode. Through a carbonization process, four heteroatoms (O, N, S, P) were self-doped into paper mulberry (PM) to obtain the carbonized material (PMC), which was then treated with KOH as an activator to prepare PMACs rich in macropores, mesopores, and micropores (Figure 5). The micropores provided a large number of active sites for carrier adsorption, while the mesopores facilitated ion diffusion kinetics by providing abundant channels that could eliminate diffusion barriers. The macropores served as a reservoir for the electrolyte, thereby shortening the path for carrier transfer. Moreover, the porous structure produced by KOH activation had an ultra-high specific surface area (SSA) (1736.1 m^2 g^{-1}), which not only effectively increased the number of reversible ion adsorption active sites but also enhanced hydrophilicity of the material due to the synergistic effect of quadruple heteroatom doping, promoting charge transfer rates and, thus, improving the material's storage. Functional groups containing O and N improved the surface hydrophilicity of the carbon-based material while providing additional sites for ion binding to enhance electronic conductivity. The S atom could increase the carbon spin density and induce structural defects in the carbon material. Phosphorus in the carbon matrix could disrupt the charge uniformity and increase the asymmetric spin density. Additionally, phosphorus could cause structural distortions, enhancing the storage capacity of Zn^{2+}. All these heteroatom dopants contributed significantly to the improvement of the electrode material's capacitance. Under optimal conditions, the prepared PMACs exhibited a considerable capacitance (240.7 F g^{-1}), an excellent energy density (108.3 Wh kg^{-1}), and a competitive power density (450 W kg^{-1}). At high mass loading, they demonstrated excellent capacitance, rate performance, and impressive cycle stability (97.1% retention after 10,000 cycles at 10 A/g under a mass loading of 14.46 mg cm^{-2}). The strategy employed in this study is of great significance for the development of low-cost, environmentally friendly, and electrochemically superior active materials.

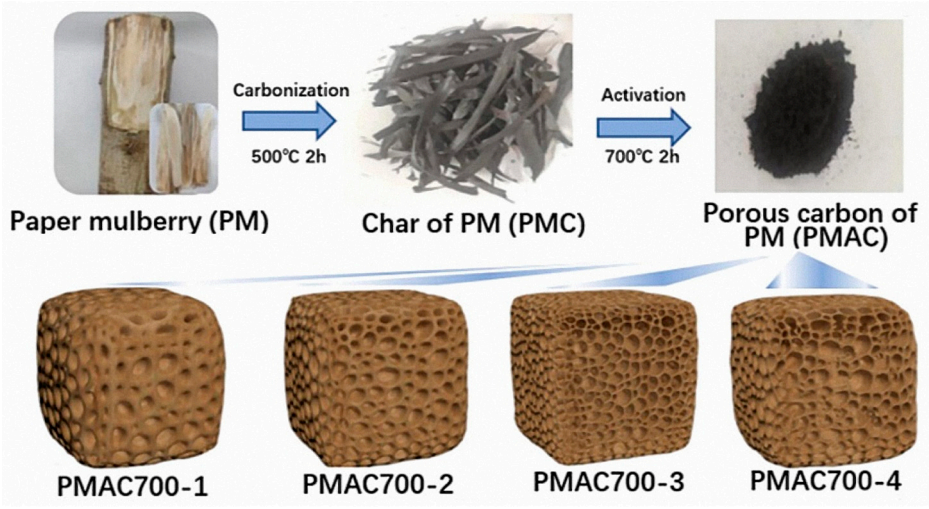

Figure 5. Schematic diagram of synthetic procedure of PMACs [95].

Graphene's enormous theoretical SSA, excellent conductivity, and chemical stability are considered promising for energy storage applications as an alternative material [96]. However, the severe aggregation problem caused by the strong van der Waals forces between graphene layers leads to significant barriers between the graphene layers, which severely reduces the actual SSA and conductivity of graphene [97]. Yao et al. [98] prepared a novel 3D phosphorus-doped carbon nanotube/reduced graphene oxide (P–CNT/rGO) composite aerogel using CNTs as intercalants and phosphoric acid as a phosphorus source through a simple one-step hydrothermal method and used it as the cathode material for Zn-HSC (Figure 6). The obtained P–CNT/rGO composite aerogel retained 45.5% of its capacitance at an ultra-high current density (Dc) of 100 A/g compared to 0.1 A/g. The group also compared the specific capacitance of the P–CNT/rGO composite aerogel (213.4 F/g) with that of rGO (105.9 F/g) and CNT/rGO (144.1 F/g) at 0.5 A/g. The excellent electrochemical performance of P–CNT/rGO could be attributed to the combined effects of carbon nanotube insertion and P doping modification, which led to improvements in SSA, expansion of interlayer spacing, and enhancement of pseudocapacitive reactions. The insertion and dispersion of carbon nanotubes between graphene sheets effectively prevented the aggregation of graphene. The synergistic effect of carbon nanotube insertion and P doping modification resulted in the P–CNT/rGO having the richest micropores and mesopores, increasing the SSA of graphene. Furthermore, since the atomic radius of the P atom is larger than that of the C atom and the electronegativity of the P atom is lower than that of the C atom, the incorporation of P atoms provided more structural defects for P–CNT/rGO and altered the charge density of graphene. The functionalization of the graphene surface (P, O atoms) could improve the wettability of the electrode with the electrolyte and the surface reactivity, providing more active sites for the chemisorption/desorption of Zn^{2+} and resulting in additional pseudocapacitance that significantly enhanced the capacitance performance of graphene. The zinc-ion supercapacitor assembled with P–CNT/rGO under optimal conditions exhibited a high energy density of 92.7 Wh/kg at a power density of 80 W/kg, a power density of 80 kW/kg at an energy density of 42.2 Wh/kg, and a capacitance retention rate of 94.2% after more than 10,000 cycles at 3 A/g, demonstrating very superior stability. This strategy provides valuable references for the in-depth optimization of energy density and power density of graphene-based cathode zinc-ion supercapacitors.

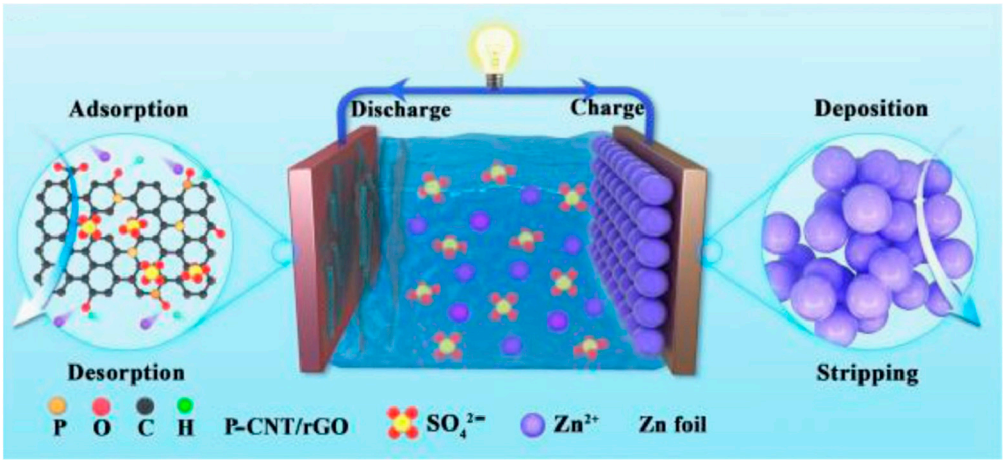

Figure 6. Schematic illustration of energy storage mechanism of the P–CNT/rGO based ZHC [98].

4.2. Heterostructure Optimization Strategy Based on TMOs

Single-phase TMOs are unable to fulfill the comprehensive performance requirements of a high capacity, high-rate performance, and long-term cycle stability. It is well known that crystalline samples exhibit strong resistance to electrolyte corrosion and better cycle stability [99], while amorphous samples contain more grain boundaries and ion diffusion channels, which can enhance electrochemical activity [100]. Therefore, if electroactive materials with different crystalline phases and chemical properties are combined rationally, it becomes feasible to achieve electrochemical performance superior to that of a single TMO [101]. Peng et al. [102] synthesized $Ni_{1.5}Co_{1.5}O_4$ through a hydrothermal reaction and then treated it with NaH_2PO_2 H_2O to acidify. Impressively, with the increase in the amount of NaH_2PO_2 H_2O, $Ni_{1.5}Co_{1.5}O_4$ underwent a redox reaction with H_3P gas to form $NiCoO_2$, as well as a dual substitution reaction where metal ions were phosphated to form NiCoP and P coordinated with O to form NiCo–PO_x. A heterostructure was obtained consisting of a large number of high-crystalline NiCoP nanoparticles dispersed in an amorphous NiCo–PO_x matrix, forming a NiCoP–$NiCoO_2$/NiCo–PO_x heterostructure (Figure 7). This crystalline/amorphous heterostructure simultaneously possesses high reactivity, performance, and long-term cycle stability. The voltage of the constructed rGO//6 M KOH//NiCoP–$NiCoO_2$/NiCo–PO_x hybrid supercapacitor could be extended to 1.56 V. It exhibited a specific capacitance of 56.1 mA h g^{-1} at 1 A g^{-1} and maintained a specific capacitance of 32.8 mA h g^{-1} at a high current density of 20 A g^{-1}. It still retained 78.7% of its capacitance after 10,000 cycles. At an energy density of 800 W kg^{-1}, it achieved a power density of 44.8 W h kg^{-1}, and at a power density of 1.6 kW kg^{-1}, it had an energy density of 26.2 Wh kg^{-1}. The strategy proposed in this heterostructure demonstrated excellent electrochemical performance, providing feasible insights for the optimization of advanced materials for energy storage applications.

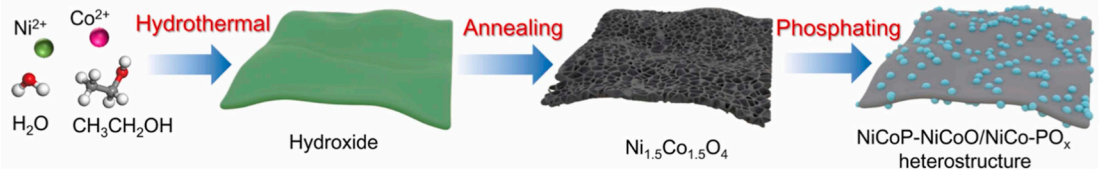

Figure 7. Schematic illustration of the synthesis procedure for NiCoP–$NiCoO_2$/NiCo–PO, heterostructure [102].

Compared to TMOs, transition metal sulfides (TMSs) have lower electronegativity and higher specific capacitance and conductivity, but they are not stable [103,104]. Transition

bi-metallic oxides (TBMOs) [105] and transition bi-metallic sulfides (TBMSs) [106] contain multiple metal ions, which can provide a richer variety of active sites for redox reactions, thus, exhibiting excellent electrochemical performance. Min et al. [107] synthesized a core–shell mesoporous heterostructure nanosheet@ $NiZn_2O_4$@$NiZn_2S_4$ (NZO@NZS) on nickel foam (NF) as a cathode material for aqueous HSCs (Figure 8). Initially, NZO nanosheets were grown on NF as a framework to increase the stability of the HSC electrode material. Subsequently, the hydrothermal method used could uniformly and interconnectedly anchor non-crystalline NZS nanosheets onto the vertically aligned NZO nanosheet framework, forming a core–shell heterostructure with larger active sites and a richer variety of active sites. This expanded ion channels and improved the electron transfer rate of the composite material, further enhancing the electrochemical performance. It is worth mentioned that the proposed synthesis method of NZO@NZS, which saved any binder, significantly improved the conductivity of the electrode material. Under optimal conditions, at a Dc of 1 A g^{-1}, NZO@NZS exhibited a high specific capacitance of 1516.0 C g^{-1}. After 10,000 cycles (Dc = 15 A g^{-1}), the capacitance retention rate remained at 86.9%. Moreover, the HSC assembled with NZO as the cathode and AC as the anode achieved an energy density of 43.4 Wh kg^{-1} at a power density of 775.0 W kg^{-1}. This research strategy provided a reasonable new direction for the design and construction of core–shell structures of TMOs.

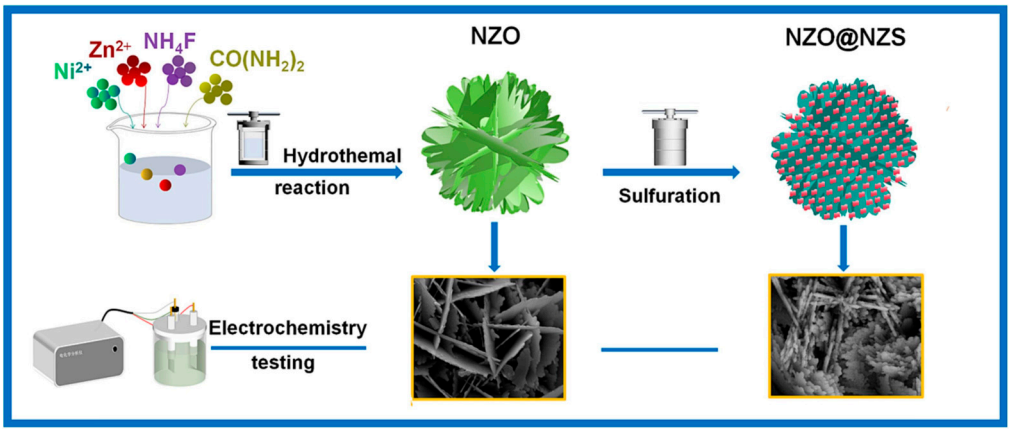

Figure 8. The fabrication process diagram of the NZO@NZS electrode [107].

4.3. Optimization Strategy of Nanocomposites Based on TMOs/Carbon Materials

Nanostructured TMOs combined with carbon-based nanomaterials (such as rGO) and non-carbon-based nanomaterials (such as MXene) to form binary or ternary nanocomposites are considered a new research direction for optimizing the electrochemical performance of HSCs.

Carbon-based materials not only improve the cycle life of TMO-based electrodes but also form a 3D network structure with TMO nanoparticles (NPs), providing an appropriate template for the growth of TMOs NPs. Ruman et al. [108] prepared SnO_2/CuO/FeO/PVP/rGO nanocomposites using a green synthesis method for use as battery-type electrode materials. The rGO sheets provided a larger conductive and porous platform for the growth of TMOs, and, thus, the obtained SnO_2/CuO/FeO/PVP/rGO exhibited significantly better electrochemical energy storage characteristics than SnO_2/CuO and SnO_2/CuO/PVP nanocomposites. Under optimal conditions, the SnO_2/CuO/FeO/PVP/rGO-modified nickel foam electrode achieved a specific capacitance of 249 C/g at 0.6 A/g. When used as a battery-type cathode with AC as the EDLC-type anode, the HSC constructed had a power density of 956 W/kg at 1.2 A/g and still retained 93.9% of its capacitance after 15,000 cycles. This group proposed a porous growth strategy, which in-

volves embedding multi-metal redox substances into conductive porous materials and has injected new vitality into the optimization of energy storage performance for future HSCs.

MXenes typically have a chemical formula of $M_{n+1}X_nT_x$ (n = 1, 2, or 3), where M represents a transition metal, X represents carbon or N, and Tx represents surface terminations such as functional groups (e.g., = O, –OH, –F, and –Cl) [109]. They exhibit significant surface redox reaction pseudocapacitance in acidic electrolytes and different pseudocapacitance based on ion insertion mechanisms in neutral and alkaline electrolytes [110], making them widely applicable in HSCs. Ti_3C_2, as one of the lightest members of the MXene family, stands out among many MXenes. Pradeepa et al. [111] synthesized a heterostructured titanium carbide–zirconium oxide nanocomposite (Ti_3C_2–ZrO_2 NC) (Figure 9) and then precisely assembled a solid-state hybrid supercapacitor device (SHSC) using Ti_3C_2–ZrO_2 NC as the cathode, AC as the anode, Whatman filter paper as the separator, and PVA–KOH gel as the solid–state electrolyte. The synergistic interaction between the typical layered structure of Ti_3C_2 and ZrO_2 nanoparticles not only promoted the interlayer ion insertion/extraction rate but also provided a sufficient number of electrochemically active sites for surface redox reactions. Moreover, the mesoporous structure of Ti_3C_2–ZrO_2 NC facilitated the effective permeation of ions through the surface. This allowed Ti_3C_2–ZrO_2 NC to exhibit excellent charge transfer kinetics and high specific capacitance compared to single Ti_3C_2 and ZrO_2 NPs. The GCD curves of the Ti_3C_2–ZrO_2 NC electrode showed nonlinear behavior, revealing its battery charge storage process, with a high specific capacitance of 483.6 C/g at 1 A/g Dc, and it still retained a capacitance retention rate as high as 88.85% after 5000 charge–discharge cycles. The assembled Ti_3C_2–ZrO_2//AC solid-state hybrid supercapacitor (SHSC) device had an energy density and power density of 75.60 Wh/kg and 1445 W/kg, respectively. The strategy proposed in this two-dimensional layered MXene structure, which plays a key role in enhancing conductivity and reaction kinetics, may become a promising battery-type material for application in future energy storage devices.

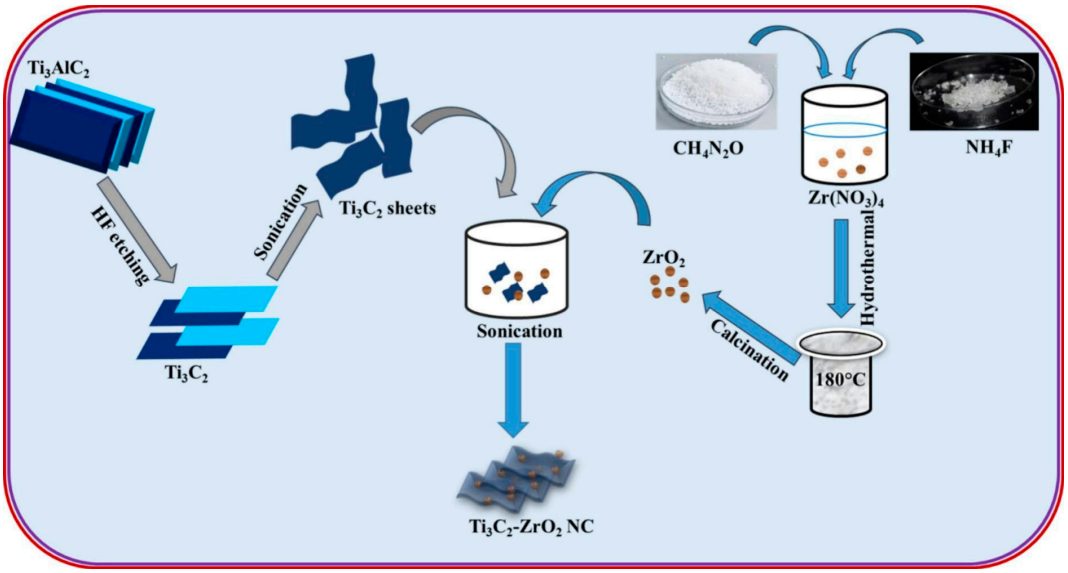

Figure 9. Schematic illustration for the synthesis procedure of TisC_2–ZrO_2 NC [111].

Unfortunately, the synthesis and processing of nanomaterials generally require specialized equipment and intricate fabrication techniques, which significantly increase the complexity and difficulty of manufacturing. Traditional metal oxide preparation often involves the mixing of hydroxides followed by high-temperature calcination/annealing/sintering processes, which are time-consuming. For instance, the synthesis of metal oxides from tin-

based mixed hydroxides requires at least 2 h of reaction time. Therefore, the development of simple and efficient nanocomposite synthesis processes is also a key focus of research, aiming to transition technology towards industrialization and commercialization. To achieve a rapid reaction time of only 30 s, Sahoo et al. [112] employed a microwave method with a commercial microwave oven. During this short period, oxidized graphite was exfoliated and reduced to rGO, while the dehydration of $CoSn(OH)_6$ formed oxide nanoparticles that were deposited on the surface of the oxidized graphene. The microwave-prepared Co_3O_4/SnO_2/rGO (CSO–rGO) ternary nanocomposite constructed a hybrid electrode with a high specific capacitance (146.4 C/g) and exceptional cycle stability (103.2% after 15,000 cycles). Additionally, the group constructed an aqueous HSC using microwave-prepared rGO as the anode, due to the porous network structure of the CSO-rGO composite materials, as well as the gradual activation and electrochemical reconstruction of the composite electrodes during cycling, there is an increase charge storage, with the device achieving a maximum energy density of 27 Wh/kg and a cycle stability of 102.4% after 10,000 cycles.

4.4. Optimization Strategy of MOF-Derived TMOs/Carbon

Metal–organic frameworks (MOFs), also known as porous coordination polymers, are inorganic–organic hybrid materials formed by the self-assembly of metal ions or clusters with organic ligands through coordination bonds, possessing molecular-level porosity. In recent years, MOF-derived materials have received extensive research in the fields of electrochemical energy storage conversion. They can not only provide crucial supporting structures for a variety of electrode materials but also offer more active sites, larger SSA, and better promotion of electrochemical reactions due to their dispersed metal components, ultra-high surface area, and controllable porosity. Among them, MOF-derived electrode materials have received widespread attention in the field of energy storage.

Bhosale et al. [113] obtained a bimetallic MOF ($CoFe_2$–MOF) through simple thermal treatment. Impressively, they directly prepared a nano-porous carbon (NPC) anode material and a binary TMO ($CoFe_2O_4$) cathode material using a single bimetallic $CoFe_2$–MOF as the sole precursor through a method called "one-for-all". An HSC was constructed using 2 M potassium hydroxide as the alkaline aqueous electrolyte. Under optimal conditions, the constructed HSC exhibited an excellent specific capacitance at a Dc of 2 mA cm^{-2}, with an energy density of 56.2 Wh kg^{-1} and a power density of 1091.5 W kg^{-1}. Moreover, it showed an outstanding cycle stability of 97.91% over 5000 GCD cycles. The revolutionary "one-for-all" concept proposed by this strategy has created endless possibilities for developing the next generation of supercapacitors with high safety, low cost, wide voltage window, and long-term cycle stability.

Tin dioxide (SnO_2) and its derivatives have been widely used as anode materials for lithium-ion supercapacitors due to their high theoretical capacity, low working potential, abundant reserves, and environmental friendliness [114,115]. The storage mechanism of lithium in SnO_2 is typically divided into two stages. The first stage is an irreversible conversion reaction, where Li^+ ions react with SnO_2 to form metallic tin (Sn) and lithium oxide (Li_2O) [116]. The second stage involves an alloy reaction between Sn and Li^+ ions, providing higher capacity. Unfortunately, the volume expansion (approximately 260%) caused by the alloy formation severely affects the lifespan of the lithium-ion supercapacitor. Duan et al. [117] synthesized a Mn_2SnO_4@C anode composite material with a uniform carbon coating and rhombic structure through a two-step carbonization process and the addition of a tin source using a Mn-based metal–organic framework (Figure 10). During the charging process, the Mn_2SnO_4 undergoes an irreversible conversion reaction, and the resulting Mn and Sn are uniformly dispersed on the material surface at the atomic scale. Subsequently, The reaction between Sn and Li^+ ($Sn + xLi^+ + xe^- \rightarrow Li_xSn$ ($0 < x < 4.4$)) results

in the formation of lithium alloys. Firstly, the alloying and conversion storage mechanisms contributed to the enhancement of electrode capacity. Secondly, the uniform carbon coating encapsulation design in Mn_2SnO_4@C not only favored the improvement of conductivity and prevented particle aggregation but also effectively buffered the volume during the Sn alloying process [118]. Moreover, the incorporation of Mn into SnO_2 significantly enhanced the intrinsic conductivity compared to pure SnO_2. During cycling, the "Mn" and "Sn" elements formed different metals (Mn, Sn), lithium alloys (Li_xSn), and metal oxides (MnO, SnO_2) at various redox potentials, creating a synergistic effect that acted as a buffering framework. At different current densities, the anode's capacity retention rate exceeded 100%, and after rate tests, the anode delivered 944 mAh g^{-1} discharge capacity. Under optimal conditions, a novel lithium-ion supercapacitor was assembled using a Mn_2SnO_4@C anode and coconut shell biomass carbon (CSBC) cathode, providing an ultra-high energy density of 217.9 Wh kg^{-1} at 210 W kg^{-1} and maintaining 25.1 Wh kg^{-1} even at a high power of 21 kW kg^{-1}. The research group's application of the Mn_2SnO_4@C anode material to lithium-ion integrated circuits offers a new approach for improving the performance of the next-generation lithium-ion integrated circuits.

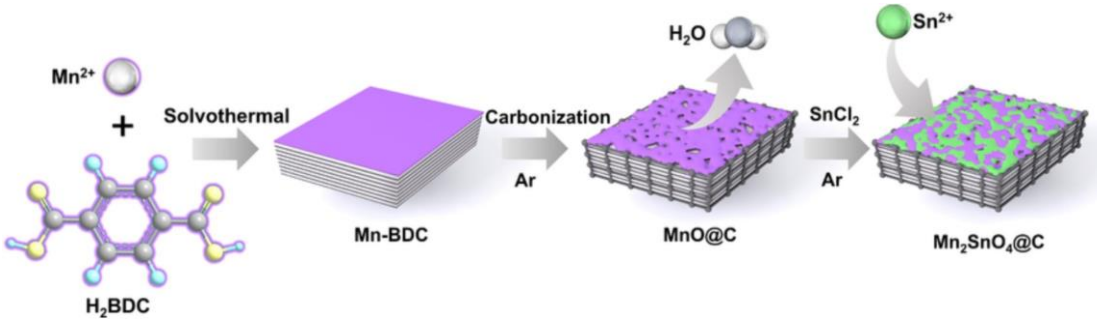

Figure 10. Schematic diagram of the synthesis route of Mn_2SnO_4@C [117].

Imidazole-based molecular sieve frameworks-8 (ZIF-8) possess a porous structure with uniformly distributed N atoms, making them an ideal precursor and template for the preparation of N-doped carbon materials [119,120]. In recent years, ZIF-8-derived N-doped porous carbons have been extensively studied and used as cathode materials for Zn-HSCs [121]. However, the limited N content in the ZIF-8 precursor has restricted the further improvement of the storage capacity of Zn-HSC. Jia et al. [122] selected a N-rich MOF (Zn-based metal-triazolate, Zn-MET) as a carbon precursor and N source, and prepared Zn-MET–x (x = pyrolysis temperature) with ultra-high N doping and hierarchical porous structures using a simple direct pyrolysis process, effectively accelerating the diffusion kinetics of zinc ions. Therefore, the optimal Zn-MET–800 used as a cathode demonstrated impressive performance. The constructed zinc-ion HSC had a high capacity of 164.2 mAh/g at 0.1 A/g and excellent rate capability of 64.4 mAh/g at 10 A/g, with a high cycle stability retention rate of 90.3% after 30,000 cycles at 10 A/g. This strategy provides a potential pathway for the preparation of advanced porous carbon materials with ultra-high N doping and offers new insights for the development of high-performance Zn-HSC.

4.5. Optimization Strategies Based on Electrolytes

The voltage window directly affects the performance and lifespan of supercapacitors. Previous studies have shown that novel electrolyte decoupling strategies can extend the voltage window, with Zhong et al. [123] using an electrolyte decoupling strategy to increase the open-circuit voltage of a Zn-MnO_2 battery from 1.50 V to 2.83 V, thereby enhancing energy density and lifespan. Additionally, electrolyte decoupling strategies can also utilize different electrolytes to replace traditional cathodes used for Zn^{2+} storage with other types

of cathodes (such as those for Li^+ storage) [47]. Based on this, Wang et al. [45] proposed a new method that fixed a Ni_3S_2/Ni_2O_3 heterojunction on N-doped carbon nanosheets (Ni_3S_2/Ni_2O_3@N–CNA) and assembled a water-based dual-ion alkaline electrolyte zinc-ion supercapacitor (Figure 11). The zinc foil anode used a mixture of $Zn(AC)_2$ and NaOH as the anodic solution, while the Ni_3S_2/Ni_2O_3@N–CNA cathode used LiOH as the cathodic solution. An anion exchange membrane (AEM) was used as a separator to prevent the mixing of Zn^{2+} and Li^+ in the anodic and cathodic solutions, which could affect the reversibility of the electrode processes. During the charge storage process, compared to Ni_2O_3, the Ni_3S_2 in the Ni_3S_2/Ni_2O_3 heterostructure has a lower Ni atomic valence state, making it easier to undergo redox reactions with OH^-. During the discharge process, the reduction–oxidation reaction of Ni atoms is accompanied by the insertion and extraction of Li^+, with the Ni_3S_2/Ni_2O_3 heterojunction not only favoring the surface pseudocapacitance generated by the adsorption of hydrated Li^+ on the Ni_3S_2 side but also the dehydration behavior of hydrated Li^+ on the Ni_3S_2 and Ni_2O_3 sides, which is beneficial for the pseudocapacitance of Li^+ insertion. Under optimal conditions, the constructed water-based dual-ion alkaline electrolyte zinc-ion supercapacitor exhibited excellent specific capacitance (236 F g^{-1}) and energy density (64.2 Wh kg^{-1}). This strategy has opened up a new pathway for the development of high-performance Zn-HSCs.

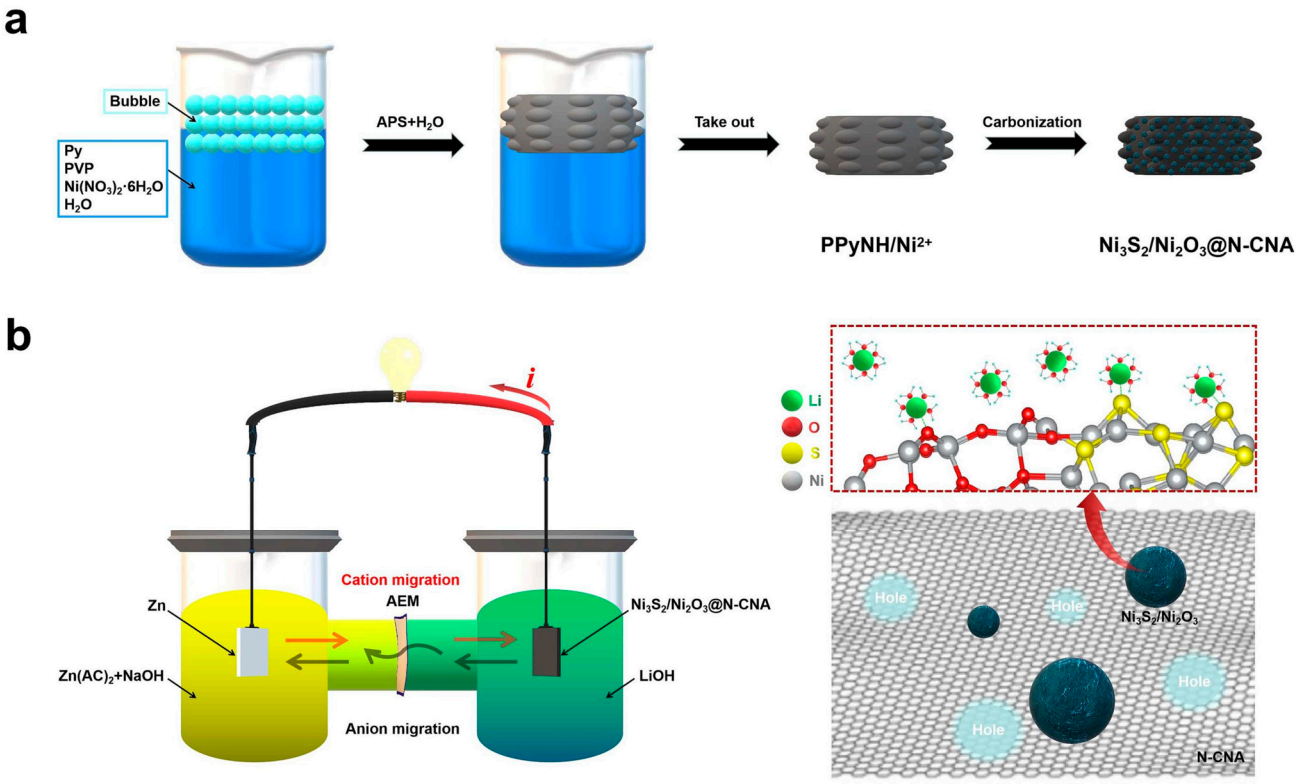

Figure 11. Schematic illustration for (**a**) the preparation process of Ni_3S_2/Ni_2O_3@N–CAN and (**b**) the charge storage mechanism of a Ni_2O_3@N–CAN //Zn Zn–HSC in the discharging process, including the device structure of the Zn–HSC (left) and the adsorption mechanism of the Ni_2O_3@N–CAN cathode for adsorbing the hydrated Li^+ ions (right) [45].

The addition of redox-active molecules to the electrolyte, which enables the storage and release of charge within the electrolyte, is another feasible strategy to enhance the specific capacitance of supercapacitors [124,125]. Due to the redox activity of thiocyanates in aqueous electrolytes and their solubility in organic solvents, Maćkowiak et al. [126] used thiocyanates as redox additives in the electrolyte. Under a current condition of C/10, they successfully achieved the insertion of thiocyanate cations into the anode using a

one-step method to assemble composite electrodes and construct a metal-ion HSC. The addition of thiocyanates compensated for the charge on the cathode and efficiently inserted metal ions into the structure of the anode. The study showed that the one-step assembly system had lower resistance than the traditional two-step assembly system, reduced assembly time and cost, and improved specific energy. Impressively, among the successfully constructed lithium-ion, sodium-ion, and potassium-ion HSCs, the Li^+-HSC with a thiocyanate electrolyte produced an exceptionally high specific energy equivalent to that of a lithium-ion battery (115 Wh kg^{-1}), which was far superior to traditional hybrid capacitors (71 Wh kg^{-1}), and it maintained efficiency above 80% of the initial capacitance even after 1000 cycles. This strategy could potentially promote further research and application of metal-ion capacitors in electrolyte optimization.

Similarly, anthraquinone compounds have received widespread attention in the preparation of redox-enhanced electrolytes [127,128]. Gan et al. [129] selected sodium anthraquinone-2-sulfonate (AQ) with high solubility, excellent stability, and unique solvation behavior as an additive to a 2 M $ZnSO_4$ aqueous solution electrolyte and constructed a zinc-ion HSC. The redox behavior of the additive originated from the reversible oxidation and reduction of the AQ/AQH_2 couple, with the conjugated electrons in the AQ molecule promoting its own redox behavior [130], and the aromatic framework enhancing the stability of the Zn anode. Additionally, the added AQ had a higher coordination binding ability with Zn^{2+} than H_2O molecules [131], effectively reducing the Zn^{2+}–H_2O interactions and enhancing the diffusion coefficient of the $ZnSO_4$–AQ system. Notably, the passivation of Zn^{2+}–additive complexes produced a robust intermediate layer with a concentration gradient, and the AQ additive also inhibited the formation of $Zn_4SO_4(OH)_6$ and ZnO by–products. The study showed that the AQ additive significantly improved the lifespan of the zinc-ion battery at 2 mA cm^{-2} and 1 mAh cm^{-2}, increasing the cycle number from 50 to 1600. Importantly, the redox behavior of the electrolyte modulated the charge transfer behavior and electrochemical kinetics of the battery. The constructed zinc-ion supercapacitor achieved a capacity of 195.0 mAh g^{-1} with 5 mM AQ, while the capacity of the ZIC without the additive was 149.6 mAh g^{-1}.

5. Conclusions and Future Perspectives

Currently, research on HSCs (Table 1) primarily focuses on the optimization of surface/interface chemistry based on TMOs and carbon-based materials, while studies on electrolytes are relatively scarce. Achieving high electron transfer and ion diffusion rates has emerged as the current research priority. Although HSC devices have made significant progress, long-term research and exploration are still required. The Zn-HSC holds great promise as a pivotal area for the further development of HSC. In terms of optimization strategies, future developments may concentrate on leveraging strategies such as heteroatom doping, pre-intercalation, nanocomposites, and binder-free approaches to develop novel pseudocapacitive materials based on TMOs, aimed at enhancing the conductivity, ion diffusion rates, and electrochemical performance of pseudocapacitive materials. Regarding the enhancement of carbon-based material properties, the main research directions are to fabricate atomically precise, reproducible, doped carbon-based materials with simple preparation processes and to develop templated carbon with a controllable three-dimensional hierarchical porous structure that matches the electrolyte ion mobility. In the industrial sector, the primary challenge in the development of HSCs is to devise methods that reduce costs and enhance sustainability. Scalable manufacturing techniques can further lower the cost of hybrid capacitors by reducing the expenses associated with electrode and electrolyte materials. For instance, Mandal et al. [132] extracted activated carbon and transition metal oxides (TMOs) from industrial energy crops such as jute, kenaf, hemp, and bamboo, which

were subsequently utilized as electrode materials for hydrogen storage capacitors. Hong et al. [133] developed a roll-to-roll dry transfer process that simultaneously controls the peeling speed and tension for large-scale production of graphene. Scaling up the production of nanocomposites to an industrial level may encounter both technical and economic challenges [134]; it is imperative to develop production processes for synthesizing efficient and selectively controlled nanocomposites to address the issues of uniformity and reproducibility encountered in batch production. Moreover, to enable flexible HSCs to operate over a wide temperature range and meet the needs of next-generation flexible, portable, and wearable electronic products, the development of flexible carbon/TMOs electrode materials and solid-state electrolytes with high ductility, self-healing ability, mechanical strength, stretchability, and compressibility is a critical issue that urgently needs to be addressed. The development of HSCs with a small volume and high energy density is also a future trend. Three-dimensional and four-dimensional 4D printing, as simple, compatible, and controllable manufacturing techniques, are essential for achieving precise and compact positioning of hybrid materials in integrated devices within limited spaces and for maximizing their performance. However, there is currently limited research on 3D and 4D printing. Bigham et al. [135] proposed 3D and 4D printing techniques for customized applications based on Mxene materials, highlighting the strong mechanical strength and biocompatibility of Mxene composites, which make them an ideal choice for scaffolding and implantable carrier applications. Incorporating both high-temperature and low-temperature performance considerations, in-depth research into the reaction kinetics and de-solvation processes of electrode materials and electrolytes, and the development of all-weather HSC with rapid charging capabilities can significantly expand application scenarios. This is a challenging yet practical research direction. Generally, at low temperatures, the reversible diffusion of lithium ions is a bottleneck affecting all-weather HSCs; while at high temperatures, the main challenges are the chemical decomposition of the electrolyte itself and the loss of surface chemical passivation mechanisms between the electrolyte and the anode/cathode interfaces.

Table 1. Performance comparison of advanced HSCs based on above electrode materials.

Sr#	Cathode Material	Anode Material	Electrolyte	Potential Window	Capacitance/ Capacity	Specific Energy [Wh kg^{-1}]	Specific Power [W kg^{-1}]	Cycling Stability [%]	Publishing Year	Refs.
1	Ni_3S_2/ Ni_2O_3@N–CNA	Zn–foil	1 M LiOH (Cathode), 0.3 M $Zn(AC)_2$ + 3 M NaOH (Anode)	0.4–1.8 V	236 F/g @1 A/g	64.2	700	75%, 10,000	2024	[45]
2	AC	T–Nb_2O_5	1 M $LiPF_6$	1.0–3.5 V	82.4 F/g @0.25 C	46.6	8400	100%, 1000	2023	[57]
3	Nd5%–Mn_2O_3 3D–MSs	AC	1 M KOH	0.0–0.55 V	862.14 F/g @0.5 A/g	32.26	800	97.3%, 2000	2020	[71]
4	Zn_xMnO_2/Ppy (ZMOP)	PCNTs	2 M $ZnSO_4$ + 0.1 M $MnSO_4$	0.0–1.9 V	109 F/g @0.1 A/g	20	867	86.4%, 5000	2024	[74]
5	CoVO–PANI@CC	AC@CC	2 M $ZnSO_4$	0.0–2.0 V	847.3 MF/cm^2 @1 mA/cm^2	1.69 mWh/cm^2	3.6 W/cm^2	81.37%, 20,000	2024	[75]
6	PMAC700–3	Zn–foil	2 M $ZnSO_4$	0.0–1.6 V	240.7 F/g @0.5 A/g	108.3	450	97.1%, 10,000	2024	[95]
7	P–CNT/rGO	Zn–foil	2 M $ZnSO_4$	0.0–1.8 V	213.4 F/g @0.5 A/g	92.7	80 KW/kg	94.2%, 10,000	2023	[98]
8	NiCoP–$NiCoO_2$/ NiCo–PO_x	RGO	6 M KOH	0.0–1.56 V	56.1 mAh/g @1 A/g	44.8	800	78.7%, 10,000	2023	[102]
9	AC	NZO@NZS	1 M KOH	0.0–0.8 V	1516 C/g @1 A/g	43.4	774.9	86.9%, 10,000	2024	[107]
10	SnO_2/CuO/FeO/ PVP/rGO	AC	2 M KOH	0.0–0.6 V	249 C/g @0.6 A/g	41.7	956	93.9%, 15,000	2024	[108]

Table 1. *Cont.*

Sr#	Cathode Material	Anode Material	Electrolyte	Potential Window	Capacitance/ Capacity	Specific Energy [Wh kg^{-1}]	Specific Power [W kg^{-1}]	Cycling Stability [%]	Publishing Year	Refs.
11	Ti_3C_2–ZrO_2 NC	AC	PVA–KOH gel	0.0–1.8 V	483.6 C/g @1 A/g	75.6	1445	88.85%, 5000	2024	[111]
12	rGO	Co_3O_4/ SnO_2/rGO (CSO–rGO)	3 M KOH	0.0–1.5 V	146.4 C/g @1 A/g	27	751.7	102.4%, 10,000	2024	[112]
13	NPC	$CoFe_2O_4$	PVA–KOH	0.0–1.4 V	112.1 F/g @1 mA/cm^2	56.2	1091.5	97.91%, 5000	2024	[113]
14	CSBC	Mn_2SnO_4@C	1 M $LiPF_6$	0.0–4.2 V	88.95 F/g @0.1 A/g	217.9	210	79%, 5000	2023	[117]
15	Zn–MET–800	Zn–foil	2 M $ZnSO_4$	0.1–1.7 V	164.2 mAh/g @0.1 A/g	128.5	4700	90.3%, 30,000	2024	[122]

Author Contributions: Conceptualization, L.G.; software, L.G. and F.L.; formal analysis, L.G.; investigation, L.G.; resources, L.G.; writing—original draft preparation, L.G. and F.L.; writing—review and editing, L.G., F.L., J.Q., W.G. and G.X.; visualization, L.G.; supervision, L.G.; project administration, L.G. and F.L.; funding acquisition, L.G., W.G. and G.X. All authors have read and agreed to the published version of the manuscript.

Funding: Liaoning Provincial Department of Education Key Scientific Research Project for Higher Education Institutions (National Project Cultivation Fund) (No. LJ212410153033), the Outstanding Youth Science Foundation of Shandong Province (Overseas) (No. 2022HWYQ-058), and National Natural Science Foundation of China (No. 22174136).

Data Availability Statement: No new data were created or analyzed in this study. Data sharing is not applicable to this article.

Conflicts of Interest: The authors declare no conflicts of interest.

References

1. Shao, Q.; Wang, P.; Huang, X. Opportunities and Challenges of Interface Engineering in Bimetallic Nanostructure for Enhanced Electrocatalysis. *Adv. Funct. Mater.* **2018**, *29*, 1806419. [CrossRef]
2. Rajagopal, A.; Yao, K.; Jen, A.K.Y. Toward Perovskite Solar Cell Commercialization: A Perspective and Research Roadmap Based on Interfacial Engineering. *Adv. Mater.* **2018**, *30*, 1800455. [CrossRef] [PubMed]
3. Wang, D.-G.; Liang, Z.; Gao, S.; Qu, C.; Zou, R. Metal-organic framework-based materials for hybrid supercapacitor application. *Coord. Chem. Rev.* **2020**, *404*, 213093. [CrossRef]
4. Kittner, N.; Lill, F.; Kammen, D.M. Energy storage deployment and innovation for the clean energy transition. *Nat. Energy* **2017**, *2*, 17125. [CrossRef]
5. Liu, J.; Wang, J.; Xu, C.; Jiang, H.; Li, C.; Zhang, L.; Lin, J.; Shen, Z.X. Advanced Energy Storage Devices: Basic Principles, Analytical Methods, and Rational Materials Design. *Adv. Sci.* **2017**, *5*, 1700322. [CrossRef]
6. Choudhary, N.; Li, C.; Moore, J.; Nagaiah, N.; Zhai, L.; Jung, Y.; Thomas, J. Asymmetric Supercapacitor Electrodes and Devices. *Adv. Mater.* **2017**, *29*, 1605336. [CrossRef] [PubMed]
7. Thackeray, M.M.; Wolverton, C.; Isaacs, E.D. Electrical energy storage for transportation—Approaching the limits of, and going beyond, lithium-ion batteries. *Energy Environ. Sci.* **2012**, *5*, 7854–7863. [CrossRef]
8. Jia, B.; Zhang, B.; Cai, Z.; Yang, X.; Li, L.; Guo, L. Construction of amorphous/crystalline heterointerfaces for enhanced electrochemical processes. *eScience* **2023**, *3*, 100112. [CrossRef]
9. Zhao, J.; Yang, L.; Li, R.; Zhou, Y. One−Step Synthesis of Fe−Based Metal–Organic Framework (MOF) Nanosheet Array as Efficient Cathode for Hybrid Supercapacitors. *Inorganics* **2023**, *11*, 169. [CrossRef]
10. Cho, S.Y.; Yoon, H.J.; Kim, N.R.; Yun, Y.S.; Jin, H.-J. Sodium-ion supercapacitors based on nanoporous pyroproteins containing redox-active heteroatoms. *J. Power Sources* **2016**, *329*, 536–545. [CrossRef]
11. Islam, M.S.; Mubarak, M.; Lee, H.-J. Hybrid Nanostructured Materials as Electrodes in Energy Storage Devices. *Inorganics* **2023**, *11*, 183. [CrossRef]
12. Ye, J.; Chen, Z.; Liu, Q.; Xu, C. Tin sulphide nanoflowers anchored on three-dimensional porous graphene networks as high-performance anode for sodium-ion batteries. *J. Colloid Interface Sci.* **2018**, *516*, 1–8. [CrossRef] [PubMed]

13. Fleischmann, S.; Leistenschneider, D.; Lemkova, V.; Krüner, B.; Zeiger, M.; Borchardt, L.; Presser, V. Tailored Mesoporous Carbon/Vanadium Pentoxide Hybrid Electrodes for High Power Pseudocapacitive Lithium and Sodium Intercalation. *Chem. Mater.* **2017**, *29*, 8653–8662. [CrossRef]
14. Zhang, K.; Yang, X.; Li, D. Engineering graphene for high-performance supercapacitors: Enabling role of colloidal chemistry. *J. Energy Chem.* **2018**, *27*, 1–5. [CrossRef]
15. Wasiński, K.; Półrolniczak, P.; Walkowiak, M. Proof-of-concept study of a new type sodium-ion hybrid electrochemical capacitor with organic electrolyte. *Electrochim. Acta* **2018**, *259*, 850–854. [CrossRef]
16. Scaravonati, S.; Magnani, G.; Gaboardi, M.; Allodi, G.; Riccò, M.; Pontiroli, D. Electrochemical intercalation of fullerene and hydrofullerene with sodium. *Carbon* **2018**, *130*, 11–18. [CrossRef]
17. Liu, X.; Wang, H.; Cui, Y.; Xu, X.; Zhang, H.; Lu, G.; Shi, J.; Liu, W.; Chen, S.; Wang, X. High-energy sodium-ion capacitor assembled by hierarchical porous carbon electrodes derived from Enteromorpha. *J. Mater. Sci.* **2018**, *53*, 6763–6773. [CrossRef]
18. Kiran, A.S.; Shankar, E.G.; Nagaraju, M.; Yu, J.S. Binder-free phosphor-coated multiphase bismuth cobalt-selenide electrode for solar-charged quasi-solid-state hybrid supercapacitors. *Appl. Surf. Sci.* **2024**, *663*, 160174. [CrossRef]
19. Mohamed, M.M.; Aziz, M.A.; Hussain, A.; Hardianto, Y.P.; Yamani, Z.H. Dendrite-free zinc-ion hybrid supercapacitor with jute-derived carbon and nanostructured zinc on steel mesh for EVs. *J. Energy Storage* **2024**, *100*, 113635. [CrossRef]
20. Junied Arbaz, S.; Chandra Sekhar, S.; Ramulu, B.; Nagaraju, M.; Su Yu, J. Electrodeposited cobalt sulfide nanolayer fenced nickel-copper carbonate hydroxide nanowires as an electrode for hybrid supercapacitors: A wind turbine-driven energy storage system for portable applications. *Appl. Surf. Sci.* **2022**, *602*, 154288. [CrossRef]
21. Vaught, L.; Sellers, R.; Shirani Bidabadi, B.; Polycarpou, A.A.; Amiri, A. Flexible zinc-ion hybrid micro-supercapacitors with polymeric current collector for integrated energy storage in wearable devices. *Chem. Eng. J.* **2024**, *492*, 152234. [CrossRef]
22. Javaid, A.; Noreen, S. Mechanically robust structural hybrid supercapacitors with high energy density for electric vehicle applications. *J. Energy Storage* **2022**, *55*, 105818. [CrossRef]
23. Jung, Y.; Pyun, K.R.; Min, J.; Yoon, H.; Lee, M.; Kim, B.-W.; Lee, J.; Ko, S.H. An Ag–Au-PANI core–shell nanowire network for visible-to-infrared data encryption and supercapacitor applications. *J. Mater. Chem. A* **2023**, *11*, 7264–7275. [CrossRef]
24. Anil Kumar, Y.; Koyyada, G.; Ramachandran, T.; Kim, J.H.; Sajid, S.; Moniruzzaman, M.; Alzahmi, S.; Obaidat, I.M. Carbon Materials as a Conductive Skeleton for Supercapacitor Electrode Applications: A Review. *Nanomaterials* **2023**, *13*, 1049. [CrossRef]
25. Zhang, Z.; Sun, S.; Xu, Z.; Yin, S. Multicomponent Hybridization Transition Metal Oxide Electrode Enriched with Oxygen Vacancy for Ultralong-Life Supercapacitor. *Small* **2023**, *19*, 2302479. [CrossRef] [PubMed]
26. Das, A.; Raj, B.; Mohapatra, M.; Andersen, S.M.; Basu, S. Performance and future directions of transition metal sulfide-based electrode materials towards supercapacitor/supercapattery. *WIREs Energy Environ.* **2021**, *11*, e414. [CrossRef]
27. Wu, C.; Deng, S.; Wang, H.; Sun, Y.; Liu, J.; Yan, H. Preparation of Novel Three-Dimensional NiO/Ultrathin Derived Graphene Hybrid for Supercapacitor Applications. *ACS Appl. Mater. Interfaces* **2014**, *6*, 1106–1112. [CrossRef] [PubMed]
28. Sheng, S.; Liu, W.; Zhu, K.; Cheng, K.; Ye, K.; Wang, G.; Cao, D.; Yan, J. Fe_3O_4 nanospheres in situ decorated graphene as high-performance anode for asymmetric supercapacitor with impressive energy density. *J. Colloid Interface Sci.* **2019**, *536*, 235–244. [CrossRef]
29. Nguyen, Q.; Nakate, U.T.; Chen, J.; Park, S.; Park, S. Ceria nanoflowers decorated Co_3O_4 nanosheets electrodes for highly efficient electrochemical supercapacitors. *Appl. Surf. Sci.* **2023**, *613*, 156034. [CrossRef]
30. Li, X.; Wang, Z.; Qiu, Y.; Pan, Q.; Hu, P. 3D graphene/ZnO nanorods composite networks as supercapacitor electrodes. *J. Alloys Compd.* **2015**, *620*, 31–37. [CrossRef]
31. Luo, L.; Meng, W.; Wang, G.; Qin, J.; He, H.; Huang, H. MnO_2 nanoflowers-decorated MXene nanosheets with enhanced supercapacitor performance. *J. Alloys Compd.* **2023**, *957*, 170411. [CrossRef]
32. Kiruthiga, R.; Nithya, C.; Karvembu, R.; Venkata, B. Reduced Graphene Oxide Embedded V_2O_5 Nanorods and Porous Honey Carbon as High Performance Electrodes for Hybrid Sodium-ion Supercapacitors. *Electrochim. Acta* **2017**, *256*, 221–231.
33. Nti, F.; Han, J.I. Layered $Na_{2/3}Ni_{1/3}Mn_{2/3}O_2$ as electrode material with two redox active transition metals for high performance supercapacitor. *J. Alloys Compd.* **2017**, *728*, 78–87. [CrossRef]
34. Niu, J.; Liang, J.; Shao, R.; Liu, M.; Dou, M.; Li, Z.; Huang, Y.; Wang, F. Tremella-like N,O-codoped hierarchically porous carbon nanosheets as high-performance anode materials for high energy and ultrafast Na-ion capacitors. *Nano Energy* **2017**, *41*, 285–292. [CrossRef]
35. Peng, M.; Wang, L.; Li, L.; Peng, Z.; Tang, X.; Hu, T.; Yuan, K.; Chen, Y. Molecular crowding agents engineered to make bioinspired electrolytes for high-voltage aqueous supercapacitors. *eScience* **2021**, *1*, 83–90. [CrossRef]
36. Bagheri, A.; Taghavi, S.; Bellani, S.; Salimi, P.; Beydaghi, H.; Panda, J.K.; Isabella Zappia, M.; Mastronardi, V.; Gamberini, A.; Balkrishna Thorat, S.; et al. Venice's macroalgae-derived active material for aqueous, organic, and solid-state supercapacitors. *Chem. Eng. J.* **2024**, *496*, 153529. [CrossRef]

37. Zhao, Y.; Hu, X.; Stucky, G.D.; Boettcher, S.W. Thermodynamic, Kinetic, and Transport Contributions to Hydrogen Evolution Activity and Electrolyte-Stability Windows for Water-in-Salt Electrolytes. *J. Am. Chem. Soc.* **2024**, *146*, 3438–3448. [CrossRef] [PubMed]
38. Zhang, P.; Zhang, W.; Wang, Z.; Wang, X.; Ren, Q.; Zhang, S.; Wang, Y.; He, L.; Liu, P.; Zhang, Q.; et al. High-voltage, low-temperature supercapacitors enabled by localized "water-in-pyrrolidinium chloride" electrolyte. *eScience* **2023**, *3*, 100184. [CrossRef]
39. Magdum, S.S.; Thangarasu, S.; Oh, T.H. Three-Dimensional Ternary rGO/VS_2/WS_2 Composite Hydrogel for Supercapacitor Applications. *Inorganics* **2022**, *10*, 229. [CrossRef]
40. Liu, S.; Luo, Z.; Tian, G.; Zhu, M.; Cai, Z.; Pan, A.; Liang, S. TiO_2 nanorods grown on carbon fiber cloth as binder-free electrode for sodium-ion batteries and flexible sodium-ion capacitors. *J. Power Sources* **2017**, *363*, 284–290. [CrossRef]
41. Loh, K.H.; Liew, J.; Liu, L.; Goh, Z.L.; Pershaanaa, M.; Kamarulazam, F.; Bashir, S.; Ramesh, K.; Ramesh, S. A comprehensive review on fundamentals and components of zinc-ion hybrid supercapacitors. *J. Energy Storage* **2024**, *81*, 110370. [CrossRef]
42. Wang, G.; Zhang, L.; Zhang, J. A review of electrode materials for electrochemical supercapacitors. *Chem. Soc. Rev.* **2012**, *41*, 797–828. [CrossRef] [PubMed]
43. Liu, Q.; Zhang, H.; Xie, J.; Liu, X.; Lu, X. Recent progress and challenges of carbon materials for Zn-ion hybrid supercapacitors. *Carbon Energy* **2020**, *2*, 521–539. [CrossRef]
44. Wang, H.; Ye, W.; Yang, Y.; Zhong, Y.; Hu, Y. Zn-ion hybrid supercapacitors: Achievements, challenges and future perspectives. *Nano Energy* **2021**, *85*, 105942. [CrossRef]
45. Wang, W.; Yang, C.; Han, D.; Yu, S.; Qi, W.; Ling, R.; Liu, G. Ni_3S_2/Ni_2O_3 heterojunction anchored on N-doped carbon nanosheet aerogels for dual-ion hybrid supercapacitors. *J. Colloid Interface Sci.* **2024**, *654*, 709–718. [CrossRef] [PubMed]
46. Zhang, D.; Li, L.; Deng, J.; Guo, S.; Pang, H.; Lu, J.; Xia, D.; Ji, X. A new type of zinc ion hybrid supercapacitor based on 2D materials. *Nanoscale* **2021**, *13*, 11004–11016. [CrossRef] [PubMed]
47. Chao, D.; Qiao, S.Z. Toward High-Voltage Aqueous Batteries: Super- or Low-Concentrated Electrolyte? *Joule* **2020**, *4*, 1846–1851. [CrossRef]
48. Jeong, J.H.; Lee, G.W.; Kim, Y.H.; Choi, Y.J.; Roh, K.C.; Kim, K.B. A holey graphene-based hybrid supercapacitor. *Chem. Eng. J.* **2019**, *378*, 122126. [CrossRef]
49. Li, B.; Dai, F.; Xiao, Q.; Yang, L.; Shen, J.; Zhang, C.; Cai, M. Nitrogen-doped activated carbon for a high energy hybrid supercapacitor. *Energy Environ. Sci.* **2016**, *9*, 102–106. [CrossRef]
50. Wang, Y.; Song, Y.; Xia, Y. Electrochemical capacitors: Mechanism, materials, systems, characterization and applications. *Chem. Soc. Rev.* **2016**, *45*, 5925–5950. [CrossRef]
51. Shao, Y.; El-Kady, M.F.; Sun, J.; Li, Y.; Zhang, Q.; Zhu, M.; Wang, H.; Dunn, B.; Kaner, R.B. Design and Mechanisms of Asymmetric Supercapacitors. *Chem. Rev.* **2018**, *118*, 9233–9280. [CrossRef] [PubMed]
52. Divya, M.L.; Praneetha, S.; Lee, Y.; Aravindan, V. Next-generation Li-ion capacitor with high energy and high power by limiting alloying-intercalation process using SnO_2@Graphite composite as battery type electrode. *Compos. Part B* **2022**, *230*, 109487. [CrossRef]
53. Dai, Y.; Chen, L.; Babayan, V.; Cheng, Q.; Saha, P.; Jiang, H.; Li, C. Ultrathin MnO_2 nanoflakes grown on N-doped carbon nanoboxes for high-energy asymmetric supercapacitors. *J. Mater. Chem. A* **2015**, *3*, 21337–21342. [CrossRef]
54. Khomenko, V.; Raymundo-Piñero, E.; Béguin, F. High-energy density graphite/AC capacitor in organic electrolyte. *J. Power Sources* **2008**, *177*, 643–651. [CrossRef]
55. Wang, H.; Wang, M.; Tang, Y. A novel zinc-ion hybrid supercapacitor for long-life and low-cost energy storage applications. *Energy Storage Mater.* **2018**, *13*, 1–7. [CrossRef]
56. Wu, S.; Chen, Y.; Jiao, T.; Zhou, J.; Cheng, J.; Liu, B.; Yang, S.; Zhang, K.; Zhang, W. An Aqueous Zn-Ion Hybrid Supercapacitor with High Energy Density and Ultrastability up to 80000 Cycles. *Adv. Energy Mater.* **2019**, *9*, 1902915. [CrossRef]
57. Ding, X.; Huang, H.; Huang, Q.; Hu, B.; Li, X.; Ma, X.; Xiong, X. Doping sites modulation of T-Nb_2O_5 to achieve ultrafast lithium storage. *J. Energy Chem.* **2023**, *77*, 280–289. [CrossRef]
58. Reddy, M.V.; Subba Rao, G.V.; Chowdari, B.V.R. Metal Oxides and Oxysalts as Anode Materials for Li Ion Batteries. *Chem. Rev.* **2013**, *113*, 5364–5457. [PubMed]
59. Liu, W.; An, Y.; Zhang, X.; Wang, L.; Li, C.; Xu, Y.; Zhang, X.; Li, S.; Yi, S.; Gong, Y.; et al. General Synthesis of Graphene/Metal Oxide Heterostructures for Enhanced Lithium Storage Performance. *Adv. Funct. Mater.* **2023**, *34*, 2313274. [CrossRef]
60. Liu, W.; An, Y.; Wang, L.; Hu, T.; Lia, C.; Xu, Y.; Wang, K.; Sun, X.; Zhang, H.; Zhang, X.; et al. Mechanically flexible reduced graphene oxide/carbon composite films for highperformance quasi-solid-state lithium-ion capacitors. *J. Energy Chem.* **2023**, *80*, 68–76. [CrossRef]
61. Ma, F.; Yuan, A.; Xu, J.; Hu, P. Porous α-MoO_3/MWCNT Nanocomposite Synthesized via a Surfactant-Assisted Solvothermal Route as a Lithium-Ion-Battery High-Capacity Anode Material with Excellent Rate Capability and Cyclability. *ACS Appl. Mater. Interfaces* **2015**, *7*, 15531–15541. [CrossRef] [PubMed]

62. Xia, Q.; Zhao, H.; Du, Z.; Wang, J.; Zhang, T.; Wang, J.; Lv, P. Synthesis and electrochemical properties of MoO_3/C composite as anode material for lithium-ion batteries. *J. Power Sources* **2013**, *226*, 107–111. [CrossRef]
63. Wu, Y.P.; Rahm, E.; Holze, R. Carbon anode materials for lithium ion batteries. *J. Power Sources* **2003**, *114*, 228–236. [CrossRef]
64. Alemour, B.; Yaacob, M.H.; Lim, H.N.; Hassan, M.R. Review of Electrical Properties of Graphene Conductive Composites. *Int. J. Nanoelectron. Mater.* **2018**, *11*, 371.
65. Kinloch, I.A.; Suhr, J.; Lou, J.; Young, R.J.; Ajayan, P.M. Composites with carbon nanotubes and graphene: An outlook. *Sci. Educ.* **2018**, *362*, 547–553. [CrossRef] [PubMed]
66. Chen, S.; Liu, F.; Xiang, Q.; Feng, X.; Qiu, G. Synthesis of Mn_2O_3 microstructures and their energy storage ability studies. *Electrochimica Acta* **2013**, *106*, 360–371. [CrossRef]
67. Chidembo, A.T.; Aboutalebi, S.H.; Konstantinov, K.; Jafta, C.J.; Liu, H.K.; Ozoemena, K.I. In situ engineering of urchin-like reduced graphene oxide–Mn_2O_3–Mn_3O_4 nanostructures for supercapacitors. *RSC Adv.* **2014**, *4*, 886–892. [CrossRef]
68. Wei, W.; Cui, X.; Chen, W.; Ivey, D.G. Manganese oxide-based materials as electrochemical supercapacitor electrodes. *Chem. Soc. Rev.* **2011**, *40*, 1697–1721. [CrossRef] [PubMed]
69. Griffith, K.J.; Wiaderek, K.M.; Cibin, G.; Marbella, L.E.; Grey, C.P. Niobium tungsten oxides for high-rate lithium-ion energy storage. *Nature* **2018**, *559*, 556–563. [CrossRef]
70. Han, Y.; Heng, S.; Wang, Y.; Qu, Q.; Zheng, H. Anchoring Interfacial Nickel Cations on Single-Crystal $LiNi_{0.8}Co_{0.1}Mn_{0.1}O_2$ Cathode Surface via Controllable Electron Transfer. *ACS Energy Lett.* **2020**, *5*, 2421–2433. [CrossRef]
71. Karuppaiah, M.; Sakthivel, P.; Asaithambi, S.; Bharat, L.K.; Nagaraju, G.; Ahamad, T.; Balamurugan, K.; Yuvakkumar, R.; Ravi, G. Elevated energy density and cycle stability of α-Mn_2O_3 3D-microspheres with addition of neodymium dopant for pouch-type hybrid supercapacitors. *Electrochim. Acta* **2020**, *362*, 137169. [CrossRef]
72. Liu, T.; Chen, L.; Wang, X.; Huang, Y.; Wang, M.; Zhang, Y. Polypyrrole-coated V_2O_5 nanobelts arrays on carbon cloth for high performance zinc energy storage. *Electrochim. Acta* **2023**, *441*, 141806. [CrossRef]
73. Wang, Y.; Jiang, G.; Zhang, Z.; Chen, H.; Li, Y.; Kong, D.; Qin, X.; Li, Y.; Zhang, X.; Wang, H. Cable-like V_2O_5 Decorated Carbon Cloth as a High-Capacity Cathode for Flexible Zinc Ion Batteries. *Energy Technol.* **2022**, *10*, 2101170. [CrossRef]
74. Xue, Y.; Huo, J.; Wang, X.; Zhao, Y. Zn_xMnO_2/PPy Nanowires Composite as Cathode Material for Aqueous Zinc-Ion Hybrid Supercapacitors. *Battery Energy* **2024**, *3*, 20240035. [CrossRef]
75. Xu, Y.; Yang, X.; Li, X.; Gao, Y.; Wang, L.; Lü, W. Flexible zinc-ion hybrid supercapacitor based on Co^{2+}-doped polyaniline/V_2O_5 electrode. *J. Power Sources* **2024**, *623*, 235399. [CrossRef]
76. Yang, G.; Huang, J.; Wan, X.; Zhu, Y.; Liu, B.; Wang, J. A low cost, wide temperature range, and high energy density flexible quasi-solid-state zinc-ion hybrid supercapacitors enabled by sustainable cathode and electrolyte design. *Nano Energy* **2021**, *90*, 106500. [CrossRef]
77. Sun, Y.; Ma, H.; Zhang, X.; Liu, B.; Liu, L.; Zhang, X.; Feng, J.; Zhang, Q.; Ding, Y.; Yang, B.; et al. Salty Ice Electrolyte with Superior Ionic Conductivity Towards Low-Temperature Aqueous Zinc Ion Hybrid Capacitors. *Adv. Funct. Mater.* **2021**, *31*, 2101277. [CrossRef]
78. Zhang, W.; Zhang, R.; Shi, M.; Ma, L.; Huang, Y. Hierarchical polygon Co_3O_4 flakes/N,O-dual doped porous carbon frameworks for flexible hybrid supercapacitors. *Electrochim. Acta* **2022**, *424*, 140631. [CrossRef]
79. Zhang, H.; Liu, Q.; Fang, Y.; Teng, C.; Liu, X.; Fang, P.; Tong, Y.; Lu, X. Boosting Zn-Ion Energy Storage Capability of Hierarchically Porous Carbon by Promoting Chemical Adsorption. *Adv. Mater.* **2019**, *31*, 1904948. [CrossRef]
80. Wang, L.; Peng, M.; Chen, J.; Tang, X.; Li, L.; Hu, T.; Yuan, K.; Chen, Y. High Energy and Power Zinc Ion Capacitors: A Dual-Ion Adsorption and Reversible Chemical Adsorption Coupling Mechanism. *ACS Nano* **2022**, *16*, 2877–2888. [CrossRef]
81. Zhang, L.L.; Zhao, X.; Ji, H.; Stoller, M.D.; Lai, L.; Murali, S.; McDonnell, S.; Cleveger, B.; Wallace, R.M.; Ruoff, R.S. Nitrogen doping of graphene and its effect on quantum capacitance, and a new insight on the enhanced capacitance of N-doped carbon. *Energy Environ. Sci.* **2012**, *5*, 9618. [CrossRef]
82. Shao, Y.; Sun, Z.; Tian, Z.; Li, S.; Wu, G.; Wang, M.; Tong, X.; Shen, F.; Xia, Z.; Tung, V.; et al. Regulating Oxygen Substituents with Optimized Redox Activity in Chemically Reduced Graphene Oxide for Aqueous Zn-Ion Hybrid Capacitor. *Adv. Funct. Mater.* **2020**, *31*, 2007843. [CrossRef]
83. Xu, H.; He, W.; Li, Z.; Chi, J.; Jiang, J.; Huang, K.; Li, S.; Sun, G.; Dou, H.; Zhang, X. Revisiting Charge Storage Mechanism of Reduced Graphene Oxide in Zinc Ion Hybrid Capacitor beyond the Contribution of Oxygen-Containing Groups. *Adv. Funct. Mater.* **2022**, *32*, 2111131. [CrossRef]
84. Luo, J.; Xu, L.; Liu, H.; Wang, Y.; Wang, Q.; Shao, Y.; Wang, M.; Yang, D.; Li, S.; Zhang, L.; et al. Harmonizing Graphene Laminate Spacing and Zinc-Ion Solvated Structure toward Efficient Compact Capacitive Charge Storage. *Adv. Funct. Mater.* **2022**, *32*, 2112151. [CrossRef]
85. Wu, Z.S.; Parvez, K.; Feng, X.; Müllen, K. Graphene-based in-plane micro-supercapacitors with high power and energy densities. *Nat. Commun.* **2013**, *4*, 2487. [CrossRef] [PubMed]

86. Nagar, B.; Dubal, D.P.; Pires, L.; Merkoçi, A.; Gómez-Romero, P. Design and Fabrication of Printed Paper-Based Hybrid Micro-Supercapacitor by using Graphene and Redox-Active Electrolyte. *ChemSusChem* **2018**, *11*, 1849–1856. [CrossRef]
87. Dubal, D.P.; Chodankar, N.R.; Caban-Huertas, Z.; Wolfart, F.; Vidotti, M.; Holze, R.; Lokhande, C.D.; Gomez-Romero, P. Synthetic approach from polypyrrole nanotubes to nitrogen doped pyrolyzed carbon nanotubes for asymmetric supercapacitors. *J. Power Sources* **2016**, *308*, 158–165. [CrossRef]
88. Fan, X.; Peng, Z.; Yang, Y.; Zhou, H.; Guo, X. Atomic H-induced cutting and unzipping of single-walledcarbon nanotube carpets with teepee structure and theirenhanced supercapacitor performance. *J. Mater. Chem. A* **2015**, *3*, 10077–10084. [CrossRef]
89. Choi, C.; Lee, J.A.; Choi, A.Y.; Kim, Y.T.; Lepró, X.; Lima, M.D.; Baughman, R.H.; Kim, S.J. Flexible Supercapacitor Made of Carbon Nanotube Yarn with Internal Pores. *Adv. Mater.* **2013**, *26*, 2059–2065. [CrossRef]
90. Sun, G.; Yang, H.; Zhang, G.; Gao, J.; Jin, X.; Zhao, Y.; Jiang, L.; Qu, L. A capacity recoverable zinc-ion micro-supercapacitor. *Energy Environ. Sci.* **2018**, *11*, 3367–3374. [CrossRef]
91. Li, W.; Zhang, F.; Dou, Y.; Wu, Z.; Liu, H.; Qian, X.; Liu, D.; Xia, Y.; Tu, B.; Zhao, D. A Self-Template Strategy for the Synthesis of Mesoporous Carbon Nanofibers as Advanced Supercapacitor Electrodes. *Adv. Energy Mater.* **2011**, *1*, 382–386. [CrossRef]
92. Jost, K.; Stenger, D.; Perez, C.R.; McDonough, J.K.; Lian, K.; Gogotsi, Y.; Dion, G. Knitted and screen printed carbon-fiber supercapacitors for applications in wearable electronics. *Energy Environ. Sci.* **2013**, *6*, 2698. [CrossRef]
93. Ren, J.; Bai, W.; Guan, G.; Zhang, Y.; Peng, H. Flexible and Weaveable Capacitor Wire Based on a Carbon Nanocomposite Fiber. *Adv. Mater.* **2013**, *25*, 5965–5970. [CrossRef] [PubMed]
94. Li, H.; Wu, J.; Wang, L.; Liao, Q.; Niu, X.; Zhang, D.; Wang, K. A zinc ion hybrid capacitor based on sharpened pencil-like hierarchically porous carbon derived from metal–organic framework. *Chem. Eng. J.* **2022**, *428*, 131071. [CrossRef]
95. Li, T.; Wang, D.; Zhang, B.; Ding, P.; Li, H.; Wang, T.; Pei, Q.; Liu, X.; Guo, R. Tetra-heteroatom self-doped and hierarchical porous carbon toward high-performance zinc-ion hybrid supercapacitors. *Chem. Eng. Sci.* **2024**, *298*, 120352. [CrossRef]
96. Li, B.; Yu, M.; Li, Z.; Yu, C.; Wang, H.; Li, Q. Constructing Flexible All-Solid-State Supercapacitors from 3D Nanosheets Active Bricks via 3D Manufacturing Technology: A Perspective Review. *Adv. Funct. Mater.* **2022**, *32*, 2201166. [CrossRef]
97. Sun, Z.; Fang, S.; Hu, Y.H. 3D Graphene Materials: From Understanding to Design and Synthesis Control. *Chem. Rev.* **2020**, *120*, 10336–10453. [CrossRef] [PubMed]
98. Yao, J.; Li, F.; Zhou, R.; Guo, C.; Liu, X.; Zhu, Y. Phosphorous-doped carbon nanotube/reduced graphene oxide aerogel cathode enabled by pseudocapacitance for high energy and power zinc-ion hybrid capacitors. *Chin. Chem. Lett.* **2024**, *35*, 108354. [CrossRef]
99. Jiang, S.; Yun, S.; Cao, H.; Zhang, Z.; Feng, H.; Chen, H. Porous carbon matrix-encapsulated MnO in situ derived from metal-organic frameworks as advanced anode materials for Li-ion capacitors. *Sci. China Mater.* **2021**, *65*, 59–68. [CrossRef]
100. Huang, C.; Song, X.; Qin, Y.; Xu, B.; Chen, H.C. Cation exchange reaction derived amorphous bimetal hydroxides as advanced battery materials for hybrid supercapacitors. *J. Mater. Chem. A* **2018**, *6*, 21047–21055. [CrossRef]
101. Chen, H.C.; Qin, Y.; Cao, H.; Song, X.; Huang, C.; Feng, H.; Zhao, X.S. Synthesis of amorphous nickel–cobalt–manganese hydroxides for supercapacitor-battery hybrid energy storage system. *Energy Storage Mater.* **2019**, *17*, 194–203. [CrossRef]
102. Peng, Z.; Diao, Y.; Huang, J.; Zhang, C.; Chen, H.-C. Construction of NiCoP-NiCoO/NiCo–PO heterostructure by controllable phosphating effect for high-performance hybrid supercapacitors and alkaline zinc batteries. *J. Alloys Compd.* **2023**, *965*, 171502. [CrossRef]
103. Guo, Z.C.; Zhao, Y.X.; Mu, J.P.; Zhang, Z.X.; Mu, J.B.; Che, H.W.; Wang, Y.M.; Zhang, X.L.; Wang, G.S.; Zhang, M.Y. Fabrication of $NiPS_3$ coupled with hollow porous nitrogen-doped carbon capsules for highperformance asymmetric supercapacitor. *J. Energy Storage* **2023**, *61*, 106805. [CrossRef]
104. Wang, T.; Chen, H.C.; Yu, F.; Zhao, X.S.; Wang, H. Boosting the cycling stability of transition metal compounds-based supercapacitors. *Energy Storage Mater.* **2019**, *16*, 545–573. [CrossRef]
105. Zhai, X.; Pan, H.; Wang, F.; Gao, X.; Xiong, Z.; Li, L.; Chang, Q.; Cheng, S.; Zuo, Z.; Li, Y. Controlled Growth of 3D Interpenetrated Networks by $NiCo_2O_4$ and Graphdiyne for High-Performance Supercapacitor. *ACS Appl. Mater. Interfaces* **2022**, *14*, 18283–18292. [CrossRef]
106. Zhao, Y.; Shi, Z.; Li, H.; Wang, C.-A. Designing pinecone-like and hierarchical manganese cobalt sulfides for advanced supercapacitor electrodes. *J. Mater. Chem. A* **2018**, *6*, 12782–12793. [CrossRef]
107. Min, X.; Liu, W.-n.-y.; Wen, B.; Feng, J.; Lin, X. Nanosheet@nanosheet $NiZn_2O_4$@$NiZn_2S_4$ core-shell mesoporous heterostructure as an electrode material for aqueous hybrid supercapacitors. *J. Energy Storage* **2024**, *81*, 110410. [CrossRef]
108. Ruman, U.E.; Khan, A.; Fahad, H.M.; Asif, M.; Shaheen, F.; Aziz, M.H.; Ahmad, R.; Alam, M.; Sharif, S.; Afzal, S. Biogenic-ecofriendly synthesized SnO_2/CuO/FeO/PVP/RGO nanocomposite for enhancing energy density performance of hybrid supercapacitors. *J. Energy Storage* **2024**, *89*, 111643. [CrossRef]
109. Li, X.; Huang, Z.; Shuck, C.E.; Liang, G.; Gogotsi, Y.; Zhi, C. MXene chemistry, electrochemistry and energy storage applications. *Nat. Rev. Chem.* **2022**, *6*, 389–404. [CrossRef] [PubMed]

110. Huang, J.; Yuan, K.; Chen, Y. Wide Voltage Aqueous Asymmetric Supercapacitors: Advances, Strategies, and Challenges. *Adv. Funct. Mater.* **2021**, *32*, 2108107. [CrossRef]
111. Pradeepa, S.S.; Sutharthani, K.; Suba, D.R.; Yen, P.F.; Sivakumar, M. Two-dimensional layered Ti_3C_2 MXene nanosheets decked with ZrO_2 nanospheres for the high-performance solid-state hybrid supercapacitors. *J. Energy Storage* **2024**, *98*, 112821.
112. Sahoo, S.; Milton, A.; Sood, A.; Kumar, R.; Choi, S.; Maity, C.K.; Han, S.S. Microwave-assisted synthesis of perovskite hydroxide-derived Co_3O_4/SnO_2/reduced graphene oxide nanocomposites for advanced hybrid supercapacitor devices. *J. Energy Storage* **2024**, *99*, 113321. [CrossRef]
113. Bhosale, R.; Bhosale, S.; Chavan, V.; Jambhale, C.; Kim, D.-k.; Kolekar, S. Hybrid Supercapacitors Based on Nanoporous Carbon and $CoFe_2O_4$ Derived from a Bimetallic Organic Framework. *ACS Appl. Nano Mater.* **2024**, *7*, 2244–2257.
114. Gao, C.; Jiang, Z.; Wang, P.; Jensen, L.R.; Zhang, Y.; Yue, Y. Optimized assembling of MOF/SnO_2/Graphene leads to superior anode for lithium ion batteries. *Nano Energy* **2020**, *74*, 104868. [CrossRef]
115. Kim, H.; Kim, H.; Muhammad, S.; Um, J.H.; Sher Shah, M.S.A.; Yoo, P.J.; Yoon, W.S. Catalytic effect of reduced graphene oxide on facilitating reversible conversion reaction in SnO_2 for next-generation Li rechargeable batteries. *J. Power Sources* **2020**, *446*, 227321. [CrossRef]
116. Kebede, M.A. Tin oxide–based anodes for both lithium-ion and sodium-ion batteries. *Curr. Opin. Electrochem.* **2020**, *21*, 182–187. [CrossRef]
117. Duan, Y.K.; Li, Z.W.; Zhang, S.C.; Su, T.; Ma, Y.F.; Jiao, A.J.; Fu, Z.H. Metal-organic frameworks (MOFs)-derived Mn_2SnO_4@C anode based on dual lithium storage mechanism for high-performance lithium-ion capacitors. *Chem. Eng. J.* **2023**, *477*, 146914. [CrossRef]
118. Chen, J.S.; Lou, X.W. SnO_2-Based Nanomaterials: Synthesis and Application in Lithium-Ion Batteries. *Small* **2013**, *9*, 1877–1893. [CrossRef]
119. Wang, Q.; Sarkar, A.; Li, Z.; Lu, Y.; Velasco, L.; Bhattacharya, S.S.; Brezesinski, T.; Hahn, H.; Breitung, B. High entropy oxides as anode material for Li-ion battery applications: A practical approach. *Electrochem. Commun.* **2019**, *100*, 121–125. [CrossRef]
120. Chen, W.; Pei, J.; He, C.T.; Wan, J.; Ren, H.; Wang, Y.; Dong, J.; Wu, K.; Cheong, W.C.; Mao, J.; et al. Single Tungsten Atoms Supported on MOF-Derived N-Doped Carbon for Robust Electrochemical Hydrogen Evolution. *Adv. Mater.* **2018**, *30*, 1800396. [CrossRef] [PubMed]
121. Wei, M.; Jiang, Z.; Yang, C.; Jiang, T.; Zhang, L.; Zhao, G.; Zhu, G.; Yu, L.; Zhu, Y. A Hollow-Shaped ZIF-8-N-Doped Porous Carbon Fiber for High-Performance Zn-Ion Hybrid Supercapacitors. *Batteries* **2023**, *9*, 405. [CrossRef]
122. Jia, D.; Shen, Z.; Zhou, W.; Li, Y.; He, J.; Jiang, L.; Wei, Y.; He, X. Ultrahigh N-doped carbon with hierarchical porous structure derived from metal-organic framework for high-performance zinc ion hybrid capacitors. *Chem. Eng. J.* **2024**, *485*, 149820. [CrossRef]
123. Zhong, C.; Liu, B.; Ding, J.; Liu, X.; Zhong, Y.; Li, Y.; Sun, C.; Han, X.; Deng, Y.; Zhao, N.; et al. Decoupling electrolytes towards stable and high-energy rechargeable aqueous zinc–manganese dioxide batteries. *Nat. Energy* **2020**, *5*, 440–449. [CrossRef]
124. Byeon, J.; Ko, J.; Lee, S.; Kim, D.H.; Kim, S.W.; Kim, D.; Oh, W.; Hong, S.; Yoo, S.J. Solubility-Enhancing Hydrotrope Electrolyte with Tailor-Made Organic Redox-Active Species for Redox-Enhanced Electrochemical Capacitors. *ACS Energy Lett.* **2023**, *8*, 2345–2355. [CrossRef]
125. Evanko, B.; Boettcher, S.W.; Yoo, S.J.; Stucky, G.D. Redox-Enhanced Electrochemical Capacitors: Status, Opportunity, and Best Practices for Performance Evaluation. *ACS Energy Lett.* **2017**, *2*, 2581–2590. [CrossRef]
126. Maćkowiak, A.; Jeżowski, P.; Matsui, Y.; Ishikawa, M.; Fic, K. Redox-active electrolytes as a viable approach for the one-step assembly of metal-ion capacitors. *Energy Storage Mater.* **2024**, *65*, 103163. [CrossRef]
127. Jing, Y.; Zhao, E.W.; Goulet, M.-A.; Bahari, M.; Fell, E.M.; Jin, S.; Davoodi, A.; Jónsson, E.; Wu, M.; Grey, C.P.; et al. In situ electrochemical recomposition of decomposed redox-active species in aqueous organic flow batteries. *Nat. Chem.* **2022**, *14*, 1103–1109. [CrossRef] [PubMed]
128. Chen, Q.; Lv, Y.; Yuan, Z.; Li, X.; Yu, G.; Yang, Z.; Xu, T. Organic Electrolytes for pH-Neutral Aqueous Organic Redox Flow Batteries. *Adv. Funct. Mater.* **2021**, *32*, 2108777. [CrossRef]
129. Gan, X.; Zhang, C.; Ye, X.; Qie, L.; Shi, K. Unveiling the potential of redox electrolyte additives in enhancing interfacial stability for Zn-ion hybrid capacitors. *Energy Storage Mater.* **2024**, *65*, 103175. [CrossRef]
130. Zhao, K.; Fan, G.; Liu, J.; Liu, F.; Li, J.; Zhou, X.; Ni, Y.; Yu, M.; Zhang, Y.-M.; Su, H.; et al. Boosting the Kinetics and Stability of Zn Anodes in Aqueous Electrolytes with Supramolecular Cyclodextrin Additives. *J. Am. Chem. Soc.* **2022**, *144*, 11129–11137. [CrossRef]
131. Yu, X.; Li, Z.; Wu, X.; Zhang, H.; Zhao, Q.; Liang, H.; Wang, H.; Chao, D.; Wang, F.; Qiao, Y.; et al. Ten concerns of Zn metal anode for rechargeable aqueous zinc batteries. *Joule* **2023**, *7*, 1145–1175. [CrossRef]
132. Mandal, S.; Hu, J.; Shi, S.Q. A comprehensive review of hybrid supercapacitor from transition metal and industrial crop based activated carbon for energy storage applications. *Mater. Today Commun.* **2023**, *34*, 105207. [CrossRef]

133. Hong, N.; Kireev, D.; Zhao, Q.; Chen, D.; Akinwande, D.; Li, W. Roll-to-Roll Dry Transfer of Large-Scale Graphene. *Adv. Mater.* **2021**, *34*, 2106615. [CrossRef] [PubMed]
134. Choi, C.; Yun, T.G.; Hwang, B. Dispersion Stability of Carbon Nanotubes and Their Impact on Energy Storage Devices. *Inorganics* **2023**, *11*, 383. [CrossRef]
135. Bigham, A.; Zarepour, A.; Khosravi, A.; Iravani, S.; Zarrabi, A. 3D and 4D printing of MXene-based composites: From fundamentals to emerging applications. *Mater. Horiz.* **2024**, *11*, 6257–6288. [CrossRef]

Disclaimer/Publisher's Note: The statements, opinions and data contained in all publications are solely those of the individual author(s) and contributor(s) and not of MDPI and/or the editor(s). MDPI and/or the editor(s) disclaim responsibility for any injury to people or property resulting from any ideas, methods, instructions or products referred to in the content.